International Journal of Thermofluids 24 (2024) 100923

Contents lists available at ScienceDirect

International Journal of Thermofluids

journal homepage: www.sciencedirect.com/journal/international-journal-of-thermofluids

Artificial neural network (ANN) approach in predicting the thermo-solutal transport rate from multiple heated chips within an enclosure filled with hybrid nanocoolant

Tawsif Mahmud [a,b], Jiaul Haque Saboj [a,b], Preetom Nag [a,b,*], Goutam Saha [c], Bijan K. Saha [d]

[a] Department of Mathematics & Physics, North South University (NSU), Dhaka, 1229, Bangladesh
[b] Center of Applied & Computational Sciences (CACS), NSU, Dhaka, 1229, Bangladesh
[c] Department of Mathematics, University of Dhaka, Dhaka, 1000, Bangladesh
[d] Department of Mathematics, University of Barishal, Barishal, 8254, Bangladesh

ARTICLE INFO

Keywords:
Heated chips
Thermo-solutal convection
Artificial neural network (ANN)
Hybrid nano-coolant
Regressor model

ABSTRACT

This study focuses on enhancing heat and mass transfer in an electronic cooling system such as a rectangular cavity that contains equidistant heated chips along the bottom wall. The cavity of the present study is filled with ethylene glycol (30:70) based hybrid nano coolants of different volume fractions (ϕ) of Multi-walled Carbon Nanotube (MWCNT), Aluminum Oxide (Al_2O_3), and Copper Oxide (CuO). The set of equations controlling the thermo-solutal natural convection within the enclosure is simulated using the Galerkin weighted residual finite element method (FEM). The study has shown a good agreement of numerical results with different experimental reports within the framework of the present study. A solution space is constructed based on governing parameters such as Rayleigh number, buoyancy ratio, and Lewis number. A hybrid nano-coolant containing $\phi_{MWCNT} = 1.5$ %, $\phi_{CuO} = 0.5$ %, and $\phi_{Al2O3} = 2$ % showed a 3.11% improvement in heat transfer rate compared to the base fluid, highlighting its potential for thermal management applications. This study also investigates various machine learning models for predicting the heat and mass transfer rate, and an error analysis is conducted on the K-Nearest Neighbour Regressor, Random Forest Regressor, Decision Tree Regressor, and ANN model. The ANN model with 6-50-100-50-2 architecture showcases the best fit with the mean squared error of 0.8923 and an R^2 value of 99.96 % on testing data. The ANN model exhibits its capability to predict heat transfer and mass transfer rates within the error ranges from 1–2 % and 2–3 %, respectively, even at a strong thermal buoyancy force ($Ra = 10^5$). This accuracy showcases a novel use of ANN to efficiently predict thermo-fluidic transport behaviors of hybrid nanofluids, offering a faster alternative to resource-intensive simulations. The present study opens new possibilities for real-time, cost-effective cooling solutions, particularly in microelectronics and renewable energy, while maintaining high prediction accuracy by integrating machine learning with the nanotechnology approach.

1. Introduction

Thermo-solutal natural convection (TSNC) is an intriguing study area because of its widespread occurrence and significant impact on fluid flow and thermal and solutal transfer processes. It is governed by thermal and solutal gradients with equal or different strengths of heat and mass diffusion processes and is therefore also known as double-diffusive natural convection (DDNC). TSNC can lead to complex flow patterns and affect heat transfer (HT) rate from the active wall, making it an area of ongoing interest for the scientific community. Investigating DDNC can yield valuable insights for improving HT efficiency and breeding new HT fluids with superior performance for practical applications such as thermal energy storage, solar thermal systems, HVAC (heating, ventilation, and air conditioning) systems, and advanced cooling technologies [1,2]. In this realm, Costa et al. [3] investigated DDNC in enclosures with a parallelogram and moist air inside. The analysis focused on the HT and MT performance and how the Rayleigh number (*Ra*), aspect ratio, and inclination angle affect the global Nusselt (*Nu*) and Sherwood numbers (*Sh*). Teamah et al. [4] studied mixed convection (MC) in a rectangular cavity with a driven wall at the top, considering the mutual effects of solutal and thermal buoyancy. They found that the mass transfer (MT) rate is enhanced when the Lewis number (*Le*) increases, while the HT rate remains comparatively

* Corresponding author at: Department of Mathematics & Physics, North South University (NSU), Dhaka, 1229, Bangladesh.
E-mail address: preetom.nag@northsouth.edu (P. Nag).

https://doi.org/10.1016/j.ijft.2024.100923

Available online 21 October 2024

Nomenclature

X, Y	non-dimensional horizontal and vertical coordinate
U, V	non-dimensional velocity along the horizontal and vertical directions
d_p	Diameter of nanoparticle
Ra	Rayleigh number
Le	Lewis number
Ha	Hartman number
Re	Reynolds number
N	Buoyancy ratio
Nu	Nusselt Number
Sh	Sherwood number
D	Mass diffusivity, $m^2\ s^{-1}$
g	acceleration due to gravity, ms^{-2}
ANN	Artificial Neural Network

Greek symbols

ρ	density (kgm^{-3})
K	thermal conductivity ($Wm^{-2}k^{-2}$)
μ	viscosity ($kgm^{-1}s^{-1}$)
β	coefficient of thermal expansion
C_p	specific heat in constant pressure ($J.kg^{-1}.K^{-1}$)
Θ	temperature (K)
ϕ	nanoparticle volume fraction

unaffected. Xiao et al. [5] conducted a numerical study of double-diffusive MC phenomena surrounding a heated enclosing cylinder. They discovered that the average Sherwood number (Sh_{avg}) grows as the *Le* rises with a constant buoyancy ratio. Xia and Chen [6] studied DDNC heating from below in a closed cavity using the direct numerical simulation (DNS) method. They found that increasing the *Ra* enhances the convective flow, thereby increasing the average Nusselt number (Nu_{avg}) and improving HT efficiency. Moderres et al. [7] studied TSNC within an annular region defined by a square outer cylinder and a circular inner cylinder coated with a porous layer. They observed that the Nu_{avg} and Sherwood number (Sh_{avg}) increase with *Le* and *Ra*. Aghighi et al. [8] examined the DDNC of a non-Newtonian Casson fluid in a square cavity. They revealed that increasing the *Le* enhances MT significantly more than HT, indicating a more significant influence of mass diffusivity. Parveen et al. [9] examined the behavior of a (Fe_3O_4/water) ferrofluid within a lid-driven inclined wavy enclosure subject to heat generation and absorption. They found that aided thermal and solutal buoyancy forces ($N > 0$) and Richardson number (*Ri*) values enhance HT and MT. Bouras et al. [10] presented the flow of DDNC in the annular space between confocal elliptic cylinders filled with a Newtonian fluid, finding that higher *Ra* enhances natural convection, increasing HT and MT rates. Within a square cavity, Aghighi et al. [11] explored the DDNC of a non-Newtonian Casson fluid and observed that higher values of *Ra* enhance transfer rates. They also observed that a decrease in *N* weakens the flow strength and reduces HT and MT rates.

Research has found that the poor thermal conductivity of the base fluids being studied, such as ethylene glycol, water, and air, limits the potential for enhancing HT. However, using nanofluids has been shown to improve the thermal conductivity and HT rate from the active wall. An engineered suspension of nanometer-sized particles (diameters ranging from 1 to 100 nm) in the host fluid is referred to as nanofluid. In this context, nanoparticles with high thermal conductivity, such as metals, metal oxides, or carbon [12]. According to experimental studies, the effective thermal conductivity of water may be increased by 1.24 –1.78 times the host medium by including a tiny amount (2.5–7.5 %) of Cu-nanoparticles [13]. In certain instances, even 0.3 vol.% Cu-nanoparticles loaded into the host medium of ethylene glycol can increase effective thermal conductivity by 40 % [14]. Hybrid nanofluids (HNF) are an advancement of traditional nanofluids, incorporating two or more types of nanoparticles to enhance thermal properties further. Furthermore, hybrid nanofluids have shown superior thermal conductivity and HT rates compared to traditional nanofluids. This progress was underlined in a study by Armaghani et al. [15], where the use of a hybrid nanofluid consisting of Al_2O_3-Cu/H_2O in an L-shaped cavity resulted in improved HT performance. Additionally, Hasan et al. [16] examined the thermal performance of micro pin-finned heat chips. Their study emphasized the enhanced cooling processes by incorporating phase change materials. They found that both finned and non-finned heat chips with phase change materials outperform conventional air-cooling methods.

In a study by Abdullah et al. [17], a numerical model was employed to explore HT within PV panels by integrating a heated chip as a cooling mechanism. They discovered that using a combination of Al-Cu heat sink resulted in a significant temperature decrease of up to 22 °C. Selvakumar et al. [18] found that at $Ra = 10^3$, the Nu_{avg} increased by 25.12 % with a 3 % volume fraction of Al_2O_3-Cu/H_2O hybrid nanofluid compared to pure water. Kadhim et al. [19] revealed that the Darcy number, surface waviness, and effective thermal conductivity primarily influence the convective flow. They showed that the HT rate increases with higher nanoparticle volume fractions, peaking at $\phi = 0.04$. Haque et al. [20] quantified 2D transient NC HT enhancement using Al_2O_3-Cu/H_2O HNC. Notably, at $Ra = 10^5$, the uniform temperature boundary exhibits the highest Nu_{avg} of 10.04. A 25.12 % increase in the Nu_{avg} is recorded at $Ra = 10^3$ with a 3 % volume fraction. Elshazlyel et al. [21] investigated using nanofluids in solar collectors for enhanced convective HT. Experimentation with various nanofluids, including MWCNT, Al_2O_3, and hybrid MWCNT/ Al_2O_3, shows a 20 % efficiency improvement with a hybrid MWCNT/ Al_2O_3 over Al_2O_3. Using 0.5 % MWCNT/water nanofluid at 3.5 L/m achieves energy and exergy efficiency of 73.5 % and 51 %, respectively. Baghbanzad et al. [22] studied HNF made from silica nanospheres and MWCNT on heat transfer (HT). They observed that MWCNT improved HT by 23.3 %, while silica nanoparticles enhanced it by 8.8 % due to the increased thermal conductivity of the hybrid nanofluid, resulting in better HT performance and efficiency. Baby and Sundara [23] investigated HNF containing hydrogen-exfoliated graphene (HEG) and MWCNT and observed an enhancement in the convective HT coefficient of about 570 % at a nanofluid concentration of 0.005 %.

The transformative capabilities of Artificial Neural Networks (ANN) are rapidly permeating various aspects of the modern world within the evolving landscape of technology. The demand for multidisciplinary research collaboration has become crucial across multiple sectors, leading to significant advancements in money management systems, healthcare, autonomous vehicles, marketing, NLP (natural language processing), cybersecurity, and so on [24]. Moreover, artificial neural networks (ANN) have a far-reaching impact, including in fields such as fluid dynamics, where they play a critical role in modeling and predicting fluid flow patterns, contributing to the broader spectrum of advancements in today's modern world. Traditional methods often require substantial computational resources and lengthy simulation times for numerical simulations of fluid flow problems. In contrast, ANN can serve as a valuable alternative or aid in these scenarios. ANNs are recasting HT and MT predictions, speeding up simulations, and leading to more efficient thermal system designs by identifying complex patterns in large datasets. In a study by Seo et al. [25], a detailed investigation of natural convection within a long rectangular enclosure containing a heated sinusoidal cylinder was conducted. Using an ANN model, they examined a quantitative assessment of the influence of various parameters on heat transfer performance. An optimized ANN was developed by Afrand et al. [26] to predict the thermal conductivity ratio (TCR) of magnetic nanofluids. Comparative analyses revealed differences between the empirical correlation and the ANN findings compared to the experimental data,

with 5 % and 1.5 % variances, respectively.

An experimental study by Esfe et al. [27] on the ZnO-MWCNT/EG-water hybrid nanofluids conducted the development of an ANN architecture. Comparisons among the correlation outputs, ANN predictions, and experimental TCR demonstrated the accuracy and reliability of the ANN in modeling TCR data. Rostami et al. [28] used an artificial neural network (ANN) to predict the thermal conductivity of SiO_2/water-ethylene glycol hybrid nanofluids. The model achieved a strong correlation coefficient (R^2= 0.9939) and a low mean square error (MSE= 2.7547e−05), highlighting its accuracy in estimating thermal conductivity across different conditions. Faridzadeh et al. [29] found that the inclination angle and nanoparticle volume fraction significantly impact heat transfer, with an ANN model achieving a near-perfect correlation (R^2= 0.9999) between predicted and actual Nusselt numbers. The model's maximum error was 0.5829, with a mean square error of 5.37×10^{-5}. They have demonstrated that the ANN model accurately predicted cold rolling parameters, achieving average correlation coefficients of 0.947, 0.924, and 0.943 for training, testing, and validation sets, respectively. Xia et al. [30] The mean square error (MSE) for slip prediction was 4.2×10^{-4}, confirming the ANN's reliability in predicting rolling force, power, and slip in cold rolling processes. Yang et al. [31] used ANN to model thermal conductivity for MWCNTs-titania-Zinc oxide hybrid nanofluids at 25 °C–50 °C with 0.1 %-0.4 % volume fractions. Optimized with 26 neurons, the model achieved a maximum absolute error of less than 0.018 across 102 data points. Boulechfar et al. [32] simulated buoyancy-driven TSNC through a saturated porous medium within an elliptical annulus enclosure. They used three prediction methods: multi-variable polynomial regression, the group method of data handling (GMDH), and ANN to estimate HT and MT rates. The ANN method outperformed the others, with R-squared (R^2) values exceeding 0.99 for predicting *Nu* and *Sh*. Costa Rocha et al. [33] introduced and compared three distinct physics-informed deep learning techniques: ConvLSTM, CNN-LSTM, and a novel approach named Fourier Neural Operator (FNO). A recent study by Mandal et al. [34] investigated the thermo-fluidic transport process within an innovative M-shaped cavity filled with hybrid nanofluid and non-Darcian porous medium. The study revealed significant findings, including a substantial 61.01 % increase in HT rate due to specific geometric parameters such as sidewall inclination and the number and height of triangular undulations. They also used ANN to predict results from a prepared dataset. Bouzeffour [35] uses ANN to predict HT and MT coefficients in adiabatic liquid desiccant systems, building upon data from Varela et al. [36]. Their constructed ANN model performed results with R^2 values of 0.9344 and 0.9657 and MSE values of 9.0032 and 2.0414 for HT and MT coefficients, respectively. Employing an ANN architecture, a simplified heat flux model for RHC systems was developed by Verma et al. [37]. Their model incorporates mass flow rate, heat resistance, water temperature, and operative temperature to achieve high-accuracy prediction with an MSE of 0.00055 and an R^2 of 0.9984. The results emphasize the benefit of ANN in improving RHC system predictions and promoting energy-efficient building designs. In another application regarding the computational fluid dynamics (CFD) study, Kargar et al. [38] explored the application of the ANN model in cooling analysis. By using ANN in conjunction with CFD, the study improves the accuracy of predicting the cooling efficiency of electronic components with Cu-water nanofluid. Validation against CFD results shows that ANN accurately predicts cooling performance with only a 2.2 % maximum error. Recently, Prince et al. [39] examined the effects of magnetic field and *Re* on mixed convective HT, MT, and entropy generation in a trapezoidal container with two counter-rotating circular cylinders. They developed an ANN architecture, allowing them to predict various HT and fluid flow characteristics accurately. In the study of Esfe et al. [40], they found that the viscosity of the MWCNT–Al_2O_3/oil SAE40 hybrid nanofluid increased by about 35 % at 1 wt% nanoparticle concentration compared to the base fluid. The artificial neural network model showed excellent accuracy in predicting viscosity, with an R^2 value of 0.9992, demonstrating strong alignment between experimental and predicted data. Another study by Esfe et al. [41] used ANNs to predict the dynamic viscosity of MWCNT-Al2O3 (40:60)/Oil 5W50 hybrid nanofluid, showing high accuracy with errors below 2.6 %. Viscosity was highest below 5°C and decreased with increasing shear rates.

From the above literature review, it concludes that there exist no studies examining the evolution of the HT performance within the enclosure by switching the convective medium from mono-coolant to hybrid-coolant while considering the impact of buoyancy strength, the dominance of thermal buoyancy over solutal buoyancy diffusivity strength and thermal diffusivity compared to solutal diffusivity. More importantly, this study incorporates Finite Element Method (FEM), Machine Learning (ML) models, and Artificial Neural Networks (ANN) architecture to explore the thermal and solutal transport resulting from multiple heated chips within an enclosure, this study seeks to assess the predictive capability using K-Nearest Neighbors (KNN), Random Forest Regressor, Decision Tree Regressor algorithms, and an ANN model. This study introduces a novel approach that integrates high-fidelity FEM simulations with the efficient predictive capabilities of the ANN model. By developing an ANN architecture based on FEM data encompassing various values of Rayleigh number (*Ra)*, buoyancy ratio (*N)*, volume fraction (ϕ) nanoparticles, and Lewis number (*Le)*, this study aims to create a robust tool for rapid and accurate prediction of thermal and solutal exchange rates in complex systems. This approach holds the potential to significantly impact thermal management in microfluidics, electronics cooling, and other applications involving nanofluids and heated chipsets within a confined environment. This study lays the groundwork for developing advanced thermal management solutions that can enhance performance and efficiency in thermo-fluidic transport systems by establishing an effective prediction tool. The outcome of the present study will eventually help design better cooling systems and show how combining nanotechnology with a machine-learning approach can advance research in thermal management systems.

The structure of the article is designed to thoroughly analyze the problem and the methodologies employed to solve it. The next section begins with introducing the physical model, along with the governing equations and thermophysical properties that influence the thermos-solutal transport within the enclosure with multiple heated chips. Dimensionless heat and mass transfer rates are also discussed in this section. The following section discusses various Machine Learning (ML) Models and outlines their techniques for modeling, including K-Nearest Neighbors (KNN) Regressor, Decision Tree Regressor, Random Forest Regressor, and Artificial Neural Network (ANN), all of which are performed to predict thermos-solutal transport feature. In the next section, key metrics such as MSE, MAE, RMSE, and R^2 are used to assess the accuracy of the ML models. The Numerical Method and Code Validation section elaborates on the numerical procedure for CFD simulation, including the grid independence test and the code validation process. The core findings are presented in the Results and Discussion section, where the impact of critical parameters like convective buoyancy Force (*Ra*), buoyancy ratio (*N*), and Lewis number (*Le*) on thermal and solutal exchange rates is analyzed, alongside the development and performance of the ANN model. Finally, the cost-effectiveness of the ANN model is compared with traditional finite element method (FEM) simulations before concluding the paper.

2. Formulation of the problem

2.1. Physical model

The current study examines the natural convection (NC) phenomena within a rectangular enclosure containing three heated chips positioned on the bottom plane, as illustrated in Fig. 1. The enclosure has a vertical dimension labeled as H and a length of L= 8H. The chips are uniform in size, with a width of d= 0.45H along the x-direction and a height of h= 0.1H along the y-direction. It is important to note that the spacing

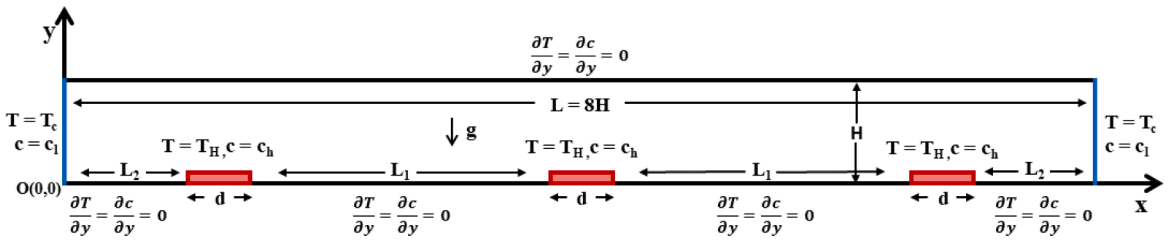

Fig. 1. Physical domain and boundary conditions.

between the chips may vary in different scenarios. Specifically, the chips are separated by a distance of $L_1 = 2.367H$. Furthermore, the separation between the first and last chips with the adjacent cold walls on both the left and right sides remains constant at $L_2 = 0.958H$.

This study investigates a base fluid comprising 30 % water and 70 % ethylene glycol (EG). The research focuses on nano-coolants, specifically studying two types: mono nano-coolants (MNC) and hybrid nano-coolants (HNC). The MNC subset includes Multi-walled carbon nanotubes (MWCNT)−EG, Aluminium Oxide (Al_2O_3)-EG, and Copper Oxide (CuO)−EG. The HNC subset consists of MWCNT- Al_2O_3-CuO-EG with a volume fraction of $\phi = 4$ %. Various proportions of MWCNT, Al_2O_3, and CuO nanoparticles are incorporated into the base fluid EG to create different HNC variants. Table 1 presents detailed information about these distinct fluids. A constant volume fraction of ϕ=4 % is maintained for all mono and hybrid nano-coolants. Moreover, different controlling factors (features) such as Ra ($10^3 \le Ra \le 10^5$), N ($0 \le N \le 4$), and Le ($1 \le Le \le 10$) are adjusted to generate the dataset used for constructing the ANN model architecture. An Artificial Neural Network (ANN) model is trained using numerical simulation data from the MNC and HNC sets and is tested using HNC 04 to assess its performance.

2.2. Governing equations

The system of the present study is described using thermal energy and concentration equations, as well as two-dimensional Navier-Stokes equations. We are considering the properties of the nano-coolants and treating the operational fluid as laminar, incompressible, and Newtonian. In addition, we estimate the buoyancy force using Boussinesq approximations, which consider density variations that occur only due to thermal and solutal gradients. The nanofluid model has been considered single-phase homogeneous with a low weight percentage($\phi \le 4$ %) of nano-constituents suspended in the host medium. The non-dimensional governing equations for our investigation are derived based on the conservation of mass, momentum, energy, and solutal [39–43].

$$\frac{\partial U}{\partial X} + \frac{\partial V}{\partial Y} = 0 \tag{1}$$

$$\frac{\rho_{HNC}}{\rho_f}\left[\frac{\partial V}{\partial t} + U\frac{\partial V}{\partial X} + V\frac{\partial V}{\partial Y}\right] = -\frac{\partial P}{\partial Y} + \frac{\mu_{HNC}}{\mu_f}\Pr\left[\frac{\partial^2 V}{\partial X^2} + \frac{\partial^2 V}{\partial Y^2}\right] + \frac{(\rho\beta)_{HNC}}{(\rho\beta)_f} Ra\ .Pr(\Theta + NC) \tag{3}$$

$$\frac{(\rho C_p)_{HNC}}{(\rho C_p)_f}\left[\frac{\partial \Theta}{\partial t} + U\frac{\partial \Theta}{\partial X} + V\frac{\partial \Theta}{\partial Y}\right] = \frac{\partial}{\partial X}\left(\frac{k_{HNC}}{k_f}\frac{\partial \Theta}{\partial X}\right) + \frac{\partial}{\partial Y}\left(\frac{k_{HNC}}{k_f}\frac{\partial \Theta}{\partial Y}\right) \tag{4}$$

$$\frac{\partial C}{\partial t} + U\frac{\partial C}{\partial X} + V\frac{\partial C}{\partial Y} = \frac{1}{Le}\left(\frac{\partial^2 C}{\partial X^2} + \frac{\partial^2 C}{\partial Y^2}\right) \tag{5}$$

The following dimensionless parameters have been utilized to obtain the non-dimensional Eqs. (1)–(5) from their corresponding dimensional equations [42,43].

$$X = \frac{x}{H}, Y = \frac{y}{H}, U = \frac{uL}{\alpha_f}, V = \frac{vL}{\alpha_f}, Ra = \frac{g\Delta TH^3\beta_f\rho_f}{\alpha_f\mu_f}, Pr = \frac{\mu_f(C_p)_f}{k_f} \tag{6}$$

$$P = \frac{pH^2}{\rho_f{\alpha_f}^2}, \Theta = \frac{T - T_c}{T_H - T_c}, C = \frac{c - c_l}{c_h - c_l}, Le = \frac{\alpha_f}{D}, \alpha_f = \frac{k_f}{(\rho C_p)_f} \tag{7}$$

The non-dimensional boundary conditions for each wall, specifying thermal, concentration, and velocity conditions, are presented in Table 2.

2.3. Thermophysical properties

The thermophysical properties of Al_2O_3, CuO, MWCNT, and the base fluid (EG) are listed in Table 3 by Mourad et al. [44], Acharya et al. [45], and Masuda et al. [46]. It is to be noted that the empirical correlation regarding the thermophysical properties of the choice of HNF is unavailable in the literature. Therefore, the present study considers the widely accepted empirical correlations for thermal conductivity and dynamic viscosity developed by Corcione et al. [47] through a regression analysis based on a wide range of experimental data (14 sets from 10 independent research groups) relevant to water or ethylene glycol-based nanofluids with particle diameters ranging from 10nm to 150nm, nanoparticle volume fraction in the range from 2–9 %, and temperature in the range between 294–324 K. Based on this model the dynamic viscosity and temperature-dependent thermal conductivity for the HNF of interest are defined in the present study. It's worth noting that the subscripts "hnc", "f", "p1", "p2", and "p3" are used throughout the study to represent the appropriate thermophysical properties of the

Table 1
Various nano-coolants with different weight percentages of nanoparticles result in different HT mediums.

Working fluids	ϕ_{MWCNT}	ϕ_{Al2O3}	ϕ_{CuO}	EG (30:70)
MWCNT-EG	4 %	0 %	0 %	96 %
CuO-EG	0 %	0 %	4 %	96 %
Al_2O_3-EG	0 %	4 %	0 %	96 %
HNC 01	2 %	1.5 %	0.5 %	96 %
HNC 02	0.5 %	2 %	1.5 %	96 %
HNC 03	1.5 %	0.5 %	2 %	96 %
HNC 04	0 %	1.33 %	2.67 %	96 %

Table 2
Boundary conditions in dimensionless form.

Boundary walls	Thermal condition	Concentration condition	Velocity condition
Top wall & Bottom wall (Excluding heated chips)	$\frac{\partial \Theta}{\partial Y} = 0$	$\frac{\partial C}{\partial Y} = 0$	$U = V = 0$
Right & left walls	$\Theta = 0$	$C = 0$	
Chips wall	$\Theta = 1$	$C = 1$	

Table 3
Thermo-physical properties of the base fluid and nanoparticles [44–46]

Properties	EG (30:70)	MWCNT	Al_2O_3	CuO
C_p (J/kg.K)	3720.5	711	773	383
k (W/m.k)	0.48547	3000	36	400
ρ (kg/m^3)	1036.6	2100	3880	8954
μ (kg/m.s)	0.0020375	–	–	–
β_T (1/K)	9.19×10^{-4}	4.2×10^{-5}	0.85×10^{-5}	1.67×10^{-5}

HNF, base fluid, MWCNT, Al_2O_3, and CuO, respectively. The effective mass density, specific heat at constant pressure, and the coefficient of thermal expansion are calculated using the mixing theory. These relationships are mathematically formulated in the following form [48]

$$\phi = \phi_{p1} + \phi_{p2} + \phi_{p3} \tag{8}$$

$$\rho_{HNC} = \phi_{p1}\rho_{p1} + \phi_{p2}\rho_{p2} + \phi_{p3}\rho_{p3} + (1-\phi)\rho_f \tag{9}$$

$$(\rho C_p)_{HNC} = \phi_{p1}\rho_{p1}C_{p_{p1}} + \phi_{p2}\rho_{p2}C_{p_{p2}} + \phi_{p3}\rho_{p3}C_{p_{p3}} + (1-\phi)\rho_f C_{p_f} \tag{10}$$

$$(\rho\beta_T)_{HNC} = \phi_{p1}(\rho\beta_T)_{p1} + \phi_{p2}(\rho\beta_T)_{p2} + \phi_{p3}(\rho\beta_T)_{p3} + (1-\phi)(\rho\beta_T)_f \tag{11}$$

$$\frac{\mu_{HNC}}{\mu_f} = \frac{1}{1 - 34.84(d_f)^{0.3} d_{hp}} \text{ where } d_f = 0.1\left(\frac{6M}{N_A \pi \rho_f}\right)^{\frac{1}{3}} \tag{12}$$

$$\frac{k_{HNC}}{k_f} = 1 + 4.4\left(\frac{2\rho_f k_b T}{\pi \mu_f d_{hp}}\right)^{0.4} Pr_f^{0.66}\left(\frac{T}{T_{fr}}\right)^{10}(k_f)^{-0.03} k_{hp} \tag{13}$$

where $M = 31.23$ g/mol is the molecular weight of the base fluids, $N_A = 6.022 \times 10^{-23}$ mol^{-1} denotes the Avogadro number, $k_b = 1.380648 \times 10^{-23}$ J/K represents the Bolzmann number, T_{fr} (= 257 K) is the freezing temperature of the host medium, and d_{hp}, k_{hp} are defined as follows

$$d_{hp} = (d_{p1})^{-0.3}(\phi_{p1})^{1.03} + (d_{p2})^{-0.3}(\phi_{p2})^{1.03} + (d_{p3})^{-0.3}(\phi_{p3})^{1.03}$$

$$k_{hp} = (k_{p1})^{0.03}(\phi_{p1})^{0.66} + (k_{p2})^{0.03}(\phi_{p2})^{0.66} + (k_{p3})^{0.03}(\phi_{p3})^{0.66}$$

The associated thermophysical quantity required for the above Eqs. (8)–(13) are listed in Table 3.

2.4. Dimensionless heat and mass transfer rate

The average of the Nusselt number (Nu_{avg}) and the Sherwood number (Sh_{avg}), which are non-dimensional quantities for the average HT and MT rate, respectively, from a heated chip and provided by the following formulas,

$$Nu_{avg} = \frac{k_{HNC}}{k_f}\left[-\frac{1}{l_w}\int \frac{\partial \Theta}{\partial \boldsymbol{n}}\, dl\right],\ Sh_{avg} = \frac{1}{l_w}\int \frac{\partial C}{\partial \boldsymbol{n}}\, dl \tag{14}$$

where the integration is evaluated over the wall of a heated chip of heated length l_w, and $\boldsymbol{n}$ denotes the direction of heat transfer normal to the heated wall. The total HT and MT rate from all three heated chips is evaluated by

$$\text{Total } Nu_{\text{avg}} = \sum_{i=1}^{3} Nu_{\text{avg}}\ , \text{Total } Sh_{\text{avg}} = \sum_{i=1}^{3} Sh_{\text{avg}} \tag{15}$$

3. Machine learning models (MLM)

The following sections discuss several regression models for machine learning approaches such as K-Nearest Neighbors (KNN), Random Forest Regressor, Decision Tree Regressor, and ANN model.

3.1. K-nearest neighbors (KNN) regressor

The K-Nearest Neighbors (KNN) can be used as a regressor by predicting the value of a target variable as the average of the k-closest points in the dataset [49]. In heat and mass transfer prediction, KNN is chosen because it's a non-parametric model that handles complex, nonlinear relationships between variables effectively, unlike traditional linear regression. This makes it particularly useful in scenarios where the physical processes, like convection or diffusion, do not follow simple linear patterns, providing more accurate predictions.

3.2. Decision tree regressor

A Decision Tree Regressor works by splitting the data into smaller subsets based on feature values, creating a tree structure to predict continuous variables. It is beneficial for predicting heat and mass transfer because it can model both linear and nonlinear relationships without needing complex data preprocessing [50]. Decision Trees efficiently handle large datasets and construct interactions between multiple parameters, making them an ideal choice when dealing with the intricate physics of thermal processes.

3.3. Random forest regressor

The Random Forest Regressor is a powerful machine-learning model that combines multiple decision trees to improve prediction accuracy. By averaging the outputs of these trees, it reduces overfitting and captures complex patterns in data. It's advantageous in predicting nonlinear relationships, like heat and mass transfer [51]. Because it handles large datasets efficiently, deals well with noisy data, and offers robust performance across varied input features. This versatility makes it a popular choice for applications where multiple variables interact dynamically.

3.4. Artificial neural network (ANN)

The human brain is a complex network of interconnected specialized cells and neurons that are responsible for processing and transmitting information. Analogously, artificial neural networks (ANNs) are a powerful tool in machine learning, designed to mimic the learning process of the human brain. Over time, ANNs have become widely recognized as an effective predictive method, often serving as a complement or even an alternative to complex computational procedures. Their ability to adapt to complex functions and diverse datasets has led to their increased prominence. ANNs can take on various forms depending on the approach and data. This study considers the supervised ANN modeling to predict *T*. Nu_{avg} and *T*. Sh_{avg} within the examined mechanism. The development, training, and post-processing of the ANN model utilized Python's Keras and Scikit-Learn libraries. Prior to the training phase, the input dataset underwent scaling using the MinMaxScaler from the Scikit-Learn library. The optimization process involved using the Adam optimizer, a fusion of two gradient descent techniques: Momentum and RMSP. It effectively adjusts the weights (w) and biases (b) to enhance model performance. The hidden layers use the Rectified Linear Unit (ReLU) activation function, which operates as follows:

$$RELU(Y) = \max(0, Y) \tag{16}$$

with inputs x_i (i= 1, 2, 3, 4,… n, where n is the number of features), the weight factor w_{ij} is applied, and part of the original signal is delivered to the network. When every input added together equals y_j, then

$$y_j = \Sigma_i^n x_i w_{ij} + b_j \tag{17}$$

The bias b_j can be used to modify the inputs. The following formulas are used by the Adam optimizer to update weights during each iteration:

$$m_t = \beta_1 m_{t-1} + (1-\beta_1)\left[\frac{\partial L}{\partial w_t}\right] \tag{18}$$

$$v_t = \beta_2 v_{t-1} + (1-\beta_2)\left[\frac{\partial L}{\partial w_t}\right]^2 \tag{19}$$

$$\underline{m} = \frac{m_t}{1-\beta_1^t} \tag{20}$$

$$\underline{v} = \frac{v_t}{1-\beta_2^t} \tag{21}$$

$$w_{t-1} = w_t + \alpha\left(\frac{\underline{m}}{\sqrt{\underline{v_t}} + \epsilon}\right) \tag{22}$$

Here,

w_t: weights at time t.	∂L: derivative of Loss Function.
w_{t-1}: weights at time t+1.	∂w_t: derivative of weights at time t.
α_t: earning rate at time t.	ε: a small positive constant.
v_t: sum of the square of past gradients.	β_1 & β_2: decay rates of average gradients.

4. Performance metrics

Prior to delving into the approach of artificial neural network (ANN) in our current study, we thoroughly analyzed several machine learning models (MLM) to ensure that the selected model could accurately predict the T. Nu_{avg} and T. Sh_{avg}. To evaluate the model selection, we chose four error metrics: Mean Square Error (MSE), Mean Average Error (MAE), Root Mean Square Error (RMSE), and R^2.

4.1. Mean squared error (MSE)

The quantity Mean Squared Error (MSE) measures the average squared difference between the predicted values and the true values, calculated by

$$MSE = \frac{1}{n}\sum_{i=1}^{n}(y_i - \widehat{y_i})^2 \tag{23}$$

where y_I, $\widehat{y_I}$, n represents the true value, predicted value, and the number of observations. MSE penalizes more significant errors than smaller ones due to the squaring of the residuals, making it particularly sensitive to outliers.

4.2. Mean absolute error (MAE)

Mean Absolute Error (MAE) quantifies the average of the magnitude differences between the predicted and true values, defined by

$$MAE = \frac{1}{n}\sum_{i=1}^{n}|y_i - \widehat{y_i}| \tag{24}$$

MAE offers a simple way to measure error by averaging the absolute differences, making it less sensitive to outliers compared to MSE. It is helpful for understanding the average size of errors in predictions.

4.3. Root mean squared error (RMSE)

Root Mean Squared Error (RMSE) is the square root of the MSE and is given by:

$$RMSE = \sqrt{\frac{1}{n}\sum_{i=1}^{n}(y_i - \widehat{y_i})^2} \tag{25}$$

RMSE has the same units as the original data, making it easier to interpret in the context of the specific problem. Like MSE, RMSE is sensitive to significant errors, as the squaring of errors accentuates them before taking the square root.

4.4. R-squared (R^2)

R-squared (R^2) is a statistical measure representing the proportion of the variance in the dependent variable that can be predicted from the independent variables, calculated by:

$$R^2 = 1 - \frac{\sum_{i=1}^{n}(y_i - \widehat{y_i})^2}{\sum_{i=1}^{n}(y_i - \overline{y})^2} \tag{26}$$

where $\overline{y}$ denotes the mean of the actual values. R^2ranges from 0 to 1, where a value closer to 1 indicates a model that explains a large proportion of the variance, and a value closer to 0 indicates a model that explains little of the variance. It is a commonly used metric to assess the goodness-of-fit of regression models.

5. Numerical method and code validation

5.1. Numerical procedure

To solve the dimensionless governing equations (Eqs. 1–5), we use the finite element method (FEM). The non-dimensional boundary conditions specified in Table 2 are taken into account. We discretize the computational domain using an unstructured triangular mesh and a set of finite elements, as shown in Fig. 2. We rigorously set the convergence criteria for the numerical simulation at 10^{-6} to ensure accuracy and solution stability. This robust method captures complex system interactions and provides accurate solutions for the studied phenomena.

The study procedure is depicted in Fig. 3, where the Computational Fluid Dynamics (CFD) simulation produces a dataset, which is then divided into train and test datasets. Subsequently, an Artificial Neural Network (ANN) architecture is designed, trained on the specified dataset, and evaluated using a validation dataset. The result is compared with other models, and the best-performing ANN model converges to an optimal configuration to effectively predict the test dataset. This iterative process ensures the development of a refined and reliable model that can comprehend and predict the intricacies of the studied system.

5.2. Grid independent test

The current study uses a grid independence test to achieve the best results with minimal computing effort and cost. The test uses MWCNT-EG and HNC01 as the working fluid for $Ra = 10^5$, $N = 4$, and $Le = 1$. According to Table 4, the optimal number of mesh elements has been found to be 11,751, as further increasing the element counts exhibits minimal effect on the $T.\ Nu_{avg}$ results. This study's findings provide valuable insights into the optimal number of elements required to produce accurate and reliable results for HT and MT characteristics. This information has the potential to reduce computation times and save computing resources while still producing dependable results.

5.3. Code validation

The code validation of the present numerical study starts by comparing the streamlined visualization with the experimental observation of the natural convection of binary gases due to horizontal thermal and solutal gradients within a square cavity [52]. The results show an excellent agreement by reproducing the experimental observations for $Ra = 5.02 \times 10^5$, $N = 0.55$ as seen in Fig. 4. Another experimental validation, as illustrated in Fig 5, is conducted for the heat transfer study within a square cavity with a single heated chip mounted from the bottom wall. Results show that the visualization of isotherms is in excellent agreement with the experimental double-exposure interferogram [53] for the case of $Ra = 1.02 \times 10^5$, and the chip height is $h = 0.25H$. In Fig. 6(a), we can compare our current research results and

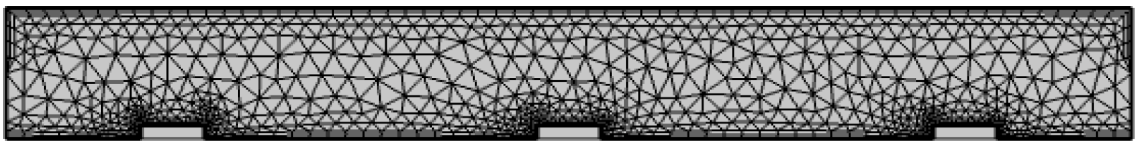

Fig. 2. Mesh configuration for the computational study.

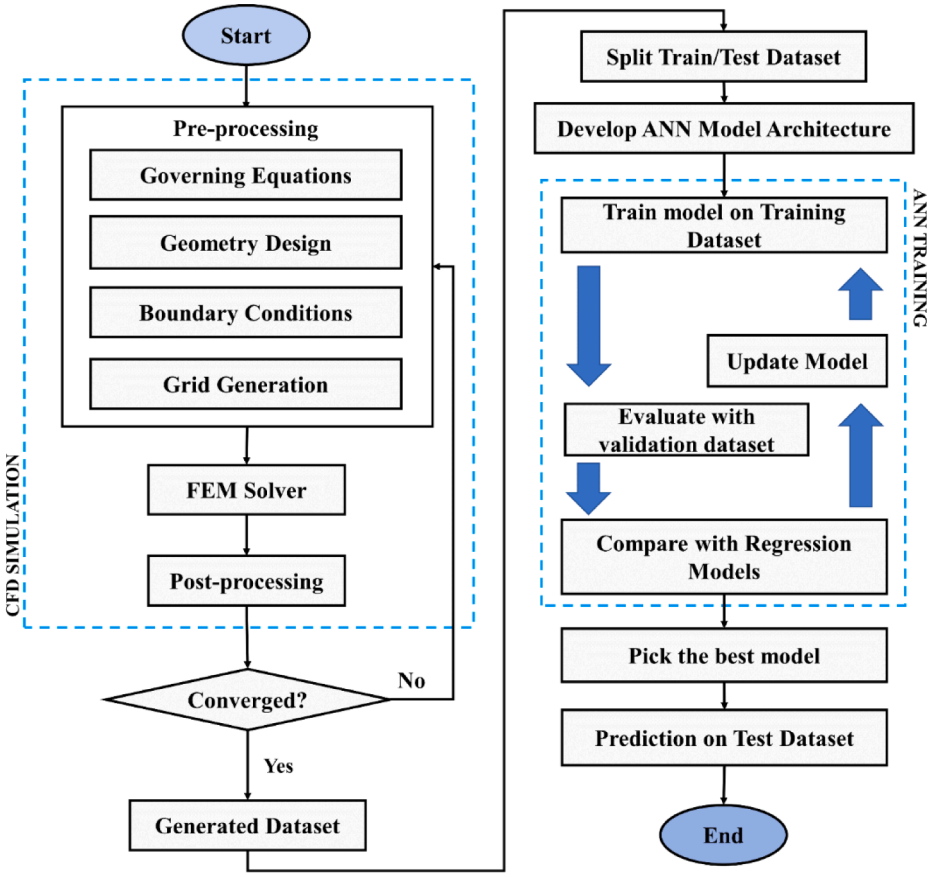

Fig. 3. Flow chart of the CFD simulation and ANN development.

Table 4
Grid Independent test on MNC (MWCNT-EG) and HNC01.

No. of elements	Total Nu_{avg}	
	MWCNT-EG	HNC01
1,703	59.16	61.05
2,636	62.17	64.22
4,196	63.93	65.93
7,758	65.59	67.64
11,751	66.36	68.41
14,239	66.46	68.55

those of Rahim et al. [54] regarding the total average Nusselt number across three heated blocks. Our numerical results resemble the findings of Rahim et al. [54], indicating a solid agreement in portraying heat transfer characteristics. This concurrence provides compelling evidence for the precision and dependability of our numerical approach in capturing the complexities of heat transfer phenomena. A verification process was conducted to ensure the reliability and accuracy of our numerical simulations concerning nanofluids, as depicted in Fig. 4(b). This verification entailed comparing our simulated results with the experimental data provided by Ho et al. [55], as well as the numerical results reported by Sheremet et al. [56] and Motlagh and Soltanipour [57], specifically for Al_2O_3-H_2O nanofluids with a 3 % volume fraction. The presented results demonstrate excellent agreement with the experimental observations and show consistency with the other set of numerical results. Additionally, Table 5 presents the results of a double-diffusive convective flow, previously studied by Sezai and Mohamad [58] and verified by Nag et al. [42]. This comparison provides further evidence for the reliability of simulating the double-diffusive convective flow in our study, where Ra ranges from 10^2 to 10^5, and double-diffusive parameters are kept constant.

6. Results and discussions

The primary objective of this study is to investigate the intricate dynamics of double-diffusive natural convective (DDNC) flow using nano-coolants as heat transfer (HT) medium in a rectangular domain containing three evenly spaced heated chips along the bottom wall. The nano-coolants consist of various weight percentage combinations of MWCNT, Al_2O_3, and CuO nanoparticles suspended in the base fluid EG (30:70), resulting in different hybrid nano-coolants (HNCs) strategically incorporated as the simulated working fluid. Extensive numerical simulations are carried out to generate a comprehensive dataset, allowing for the meticulous observation of the impact of critical parameters such as Ra ($10^3 \leq Ra \leq 10^5$), N ($0 \leq N \leq 4$), and Le ($1 \leq Le \leq 10$) on the

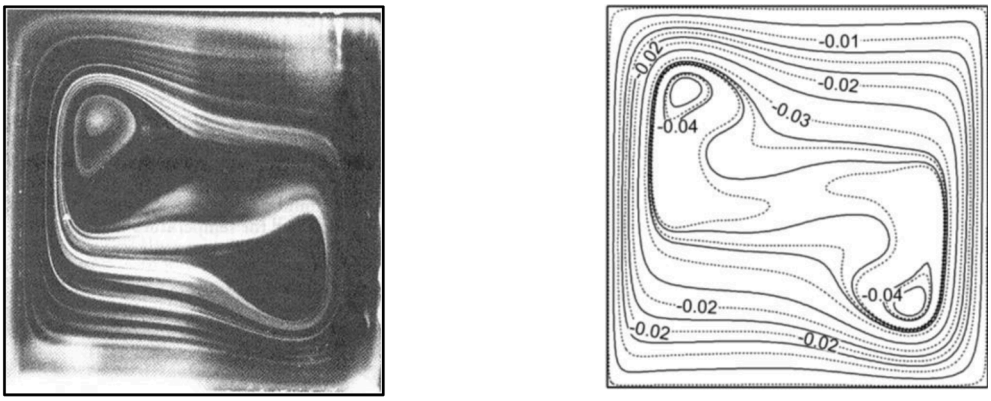

(a) Experimental observation in [52] (b) Present numerical result

Fig. 4. Validation of streamlined visualization for the thermo-solutal natural convection for binary gases reported by Weaver and Viskanta [52] and the present results for $Ra = 5.02 \times 10^5$, $N = 0.55$.

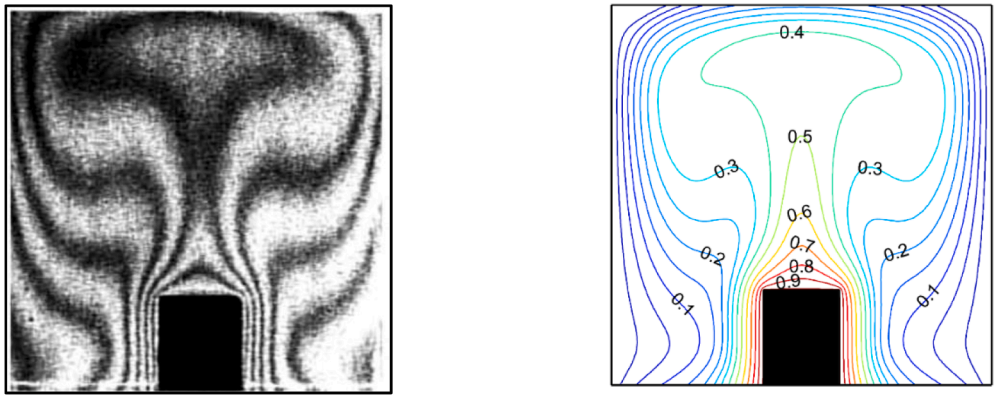

(a) Double exposure interferograms in [53] (b) Present numerical results for isotherms

Fig. 5. Validation of isothermal distribution between the experimental double-exposure interferogram [53] and the present results within a square cavity with a single heated chip for $Ra = 5.02 \times 10^5$ and $h = 0.25H$.

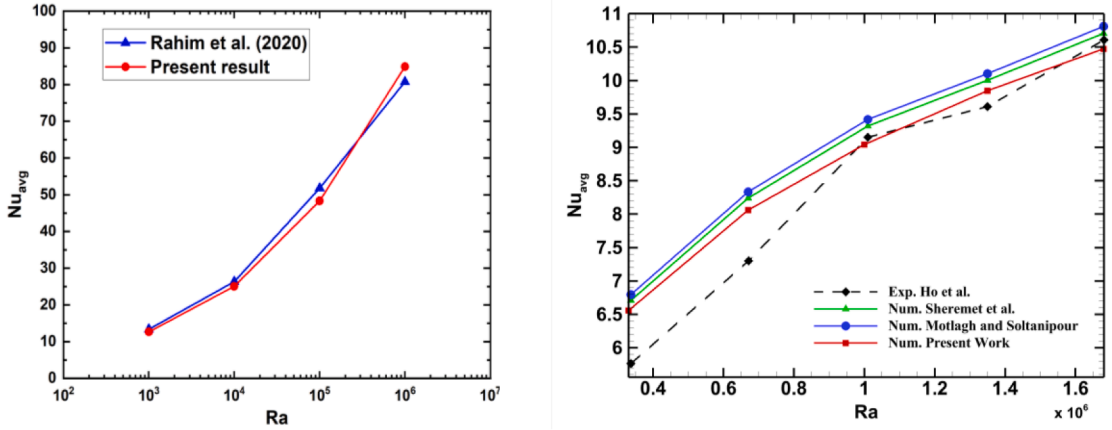

(a) (b)

Fig. 6. (a) Validation of Nu_{avg} with Rahim et al. [54] (b) Average Nusselt number (Nu_{avg}) for nanofluids with 3 % volume fraction as reported in Ho et al. [55], Sheremet et al. [56], and Motlagh and Soltanipour [57].

double-diffusive NC flow. These simulations serve as the foundation for understanding the nuanced behaviors of the HNC medium in response to varying volume fractions (ϕ=0 - 0.04) under diverse conditions. To capture the complexity of the system, an advanced ANN model is trained, leveraging various combinations of MWCNT, Al_2O_3, and CuO volume fractions within the hybrid nano-coolant. This technique enables the model to comprehend and predict the intricate interactions within the simulated fluid. The trained ANN model is also used to predict simulation outcomes, offering a computational shortcut for evaluating the system's response to varying parameters. The results are

Table 5
Comparison of *Nu* and *Sh* with Sezai and Mohamad [58] across various *Ra*, maintaining *Pr*= *Le*= 10, *N* = -0.5, and ϕ=0.0.

	Ra			
	10^2	10^3	10^4	10^5
Nu_{avg} in Sezai and Mohamad [58]	1.0057	1.0988	2.1909	4.5085
Nu_{avg} in Nag et al.[42]	1.0011	1.0866	2.1727	4.4944
Nu_{avg} in Present Study	1.0004	1.0872	2.1773	4.5173
Sh_{avg} in Sezai and Mohamad [58]	1.0589	2.4748	5.2662	....
Sh_{avg} in Nag et al.[42]	1.0421	2.4488	5.2357	10.4597
Sh_{avg} in Present Study	1.0359	2.4506	5.2749	10.658

quantitatively assessed through *T. Nu_{avg}* and *T. Sh_{avg}*, providing valuable insights into the overall HT and MT characteristics of the HNC system. This comprehensive approach combines numerical simulations with machine learning predictions to improve our understanding of double-diffusive NC with HNC, showcasing potential applications in thermal management and advanced cooling technologies.

6.1. Effect of buoyancy ratio (N) and the Lewis number (Le)

Understanding the intricate fluid motion, thermal distribution, and concentration distribution within a system is pivotal for unraveling the complexities of thermo-solutal transport phenomena. This section illustrates graphs of streamlines, isotherms, and iso-concentrations to visualize how hybrid nanofluids respond locally under various conditions. Fig. 7 illustrates the effect of the buoyancy ratio (*N*) and diffusivity ratio (*Le*) at high Rayleigh number *Ra*=10^5 on the local flow features. Specifically, subplots 7(a, b) illustrate the effect of varying *Le* (from 5 to 10) while *N* is kept constant at 2. Due to the buoyancy-driven convective HT flow, the two counter-rotating vortex cells are generated over the three heated chips within the enclosure, but the central chip leads to emanating the vortex cell. This study considered the positivity of the buoyancy ratio to observe the aiding condition of both the thermal and solutal buoyancy forces to each other. The aiding feature of the buoyancy forces lowers the boundary layer thickness along the active walls, enhancing the HT and MT features from the heated surface. The magnitude of *N*=2 indicates the strength of the thermal buoyancy force over the solutal buoyancy force by two times, intensifying flow strength and leading to densified streamlines within the intermediate regions of cold walls and nearby heated chips. The convection is observed to be weaker over the central chips, indicating weak thermo-solutal convection above the central chips compared to the other heated terminal chips. The mirroring of the contour distribution of thermal and concentration lines about the central chip indicates the observance of Rayleigh-Benard convective cells in this thermos-solutal transport study within the enclosure of interest. As seen in Fig. 7 (a,b), the increase in the LE value strengthens the thermal diffusivity over the solutal diffusivity, thereby fattening the thermal boundary layer and thinning the solutal boundary layer along the heated surface. The phenomena result in less efficient HT features relative to MT features. It is noteworthy that the effect of the *Le* variations on temperature distribution is less prominent. Still, iso-concentration lines are more directed toward the low-concentration wall with respect to increasing the diffusivity ratio *Le*. This phenomenon indicates the boosted MT feature with increasing the values of *Le*. Comparing the plots in Fig. 7 (a,b) with (c,d), one can observe that increasing *N* intensifies flow complexity and regional interactions, leading to a more intricate distribution of fluid flow, temperature, and concentration due to the greater strength of the thermal buoyancy force over the solutal one. Higher values of the buoyancy ratio (*N*=4) result in a thinner boundary layer, in which the thermos-solutal transport rate is boosted compared to a lower buoyancy ratio (*N*=2).

6.2. Thermal and solutal exchange rate

The investigation of the present study continues with the local details of the thermal exchange rate from the heated surface through the loaded nano-coolant within the enclosure. Understanding heat transfer characteristics on the surface of heated chips is crucial for optimizing thermal performance. Fig. 8 illustrates the effect of nano-coolant variation (MWCNT-EG, CuO-EG, and HNC03) on the local thermal transport rate in terms of the non-dimensional quantities such as the local Nusselt number (*Nu*). As for a particular case of aiding buoyancy forces (*N* = *4*) and equal impact of thermal to solutal diffusivity (*Le* = *1*), we present the effect of varying the strength of thermal buoyancy force by changing the values of *Ra*. Each heated chip is delineated by four distinctive points: A, B, C, and D. Analyzing local Nu across different *Ra* conditions provides insights into the detailed HT characteristics on the chip surfaces. Under all considered conditions, Chip 1 and Chip 3 consistently exhibit an asymmetric feature of HT rate, with the highest local *Nu* observed at point B and point C, respectively, which are close to the cold walls, and the thermal exchange rate is found to be extreme. Interestingly, Chip 2 always displays a distinctively lower but symmetric feature of HT rate from its surface. However, for each loaded nano-coolant within the chamber, strengthening the convective thermal buoyancy force by *Ra* leads to a boost in the thermal exchange rate from the heated surface, especially the thermal exchange rate from the central chip, contributing more significantly to the total amount, with increasing *Ra.* This detailed exploration of local *Nu* at specific chip locations offers a comprehensive understanding of the local distribution of HT from the

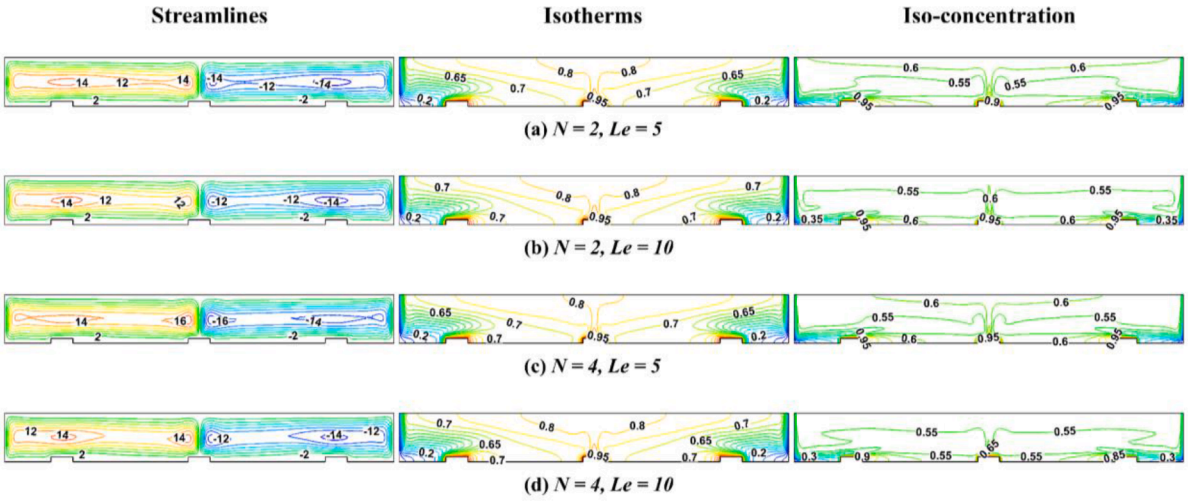

Fig. 7. Streamlines, isotherms, and iso-concentration with the variation of N and Le for Ra= 10^5 for HNC04.

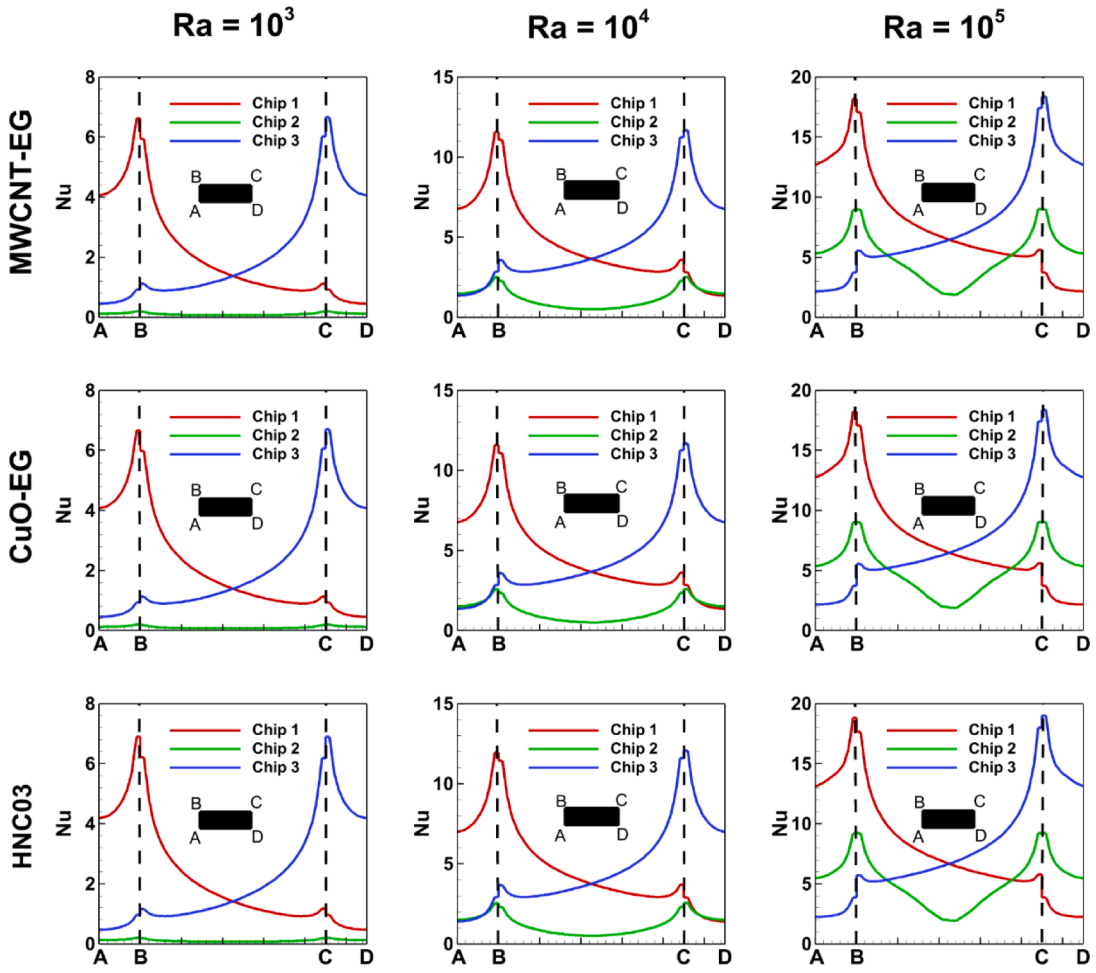

Fig. 8. Local Nu over the heated chips with different Ra values when N= 4 and Le= 1.

heated surface. It contributes to optimizing the thermal performance of the selected nanofluids. The local distribution of Nu along the heated chips shows that replacing the nano-coolant within the chamber exhibits less prominent variation qualitatively. However, nano-coolant replacement is expected to contribute to the total thermal and solutal exchange rate, as observed quantitatively in Table 6.

Table 6 shows the total average Nusselt number (*T. Nu_{avg}*) and Sherwood number (*T. Sh_{avg}*) obtained from simulations using different nanofluids at various buoyancy ratios (*N*=1, 2, 4) and Lewis numbers (*Le*= 1, 5, 10) at a constant but higher Rayleigh number (*Ra*= 10^5). Keeping the buoyancy force with constant strength, increasing the buoyancy ratio *N* from unity to higher values indicates the dominance of the thermal buoyancy force over the solutal buoyancy force by weakening it, but forces are aided towards the convective exchange rate. As a result, thermal and solutal transfer rates increase with higher values of *N*. On the other hand, raising the value of *Le* from unity to higher values indicates the dominance of thermal diffusion over solutal diffusion. Therefore, increasing *Le* leads to the thickening of the thermal boundary layer towards the decrement in the thermal exchange rate, but the thinning of the solutal boundary layer causes an increase in the solutal exchange rate. Changing the values of *N* and *Le* leads to significant variations in thermal and solutal transport efficiency among the tested

Table 6
Variation of *T. Nu_{avg}* and *T. Sh_{avg}* with different *N* and *Le* in all testing fluids when *Ra*= 10^5.

		Ra= 10^5								
		N= 1			*N*= 2			*N*= 4		
		Le= 1	*Le*= 5	*Le*= 10	*Le*= 1	*Le*= 5	*Le*= 10	*Le*= 1	*Le*= 5	*Le*= 10
MWCNT-EG	*T. Nu_{avg}*	51.67	46.34	44.89	57.72	49.151	46.57	66.36	53.75	49.32
	T. Sh_{avg}	47.98	79.79	99.44	53.47	87.59	108.64	61.35	100.23	124.03
CuO-EG	*T. Nu_{avg}*	51.827	46.48	45.015	57.89	49.35	46.73	66.60	51.06	49.57
	T. Sh_{avg}	47.926	79.796	99.452	53.42	87.59	108.69	61.34	100.27	124.18
Al_2O_3-EG	*T. Nu_{avg}*	51.41	46.09	44.64	57.45	48.96	46.37	66.08	53.644	49.18
	T. Sh_{avg}	47.85	79.66	99.276	53.36	87.42	108.53	61.26	100.187	123.98
HNC01	*T. Nu_{avg}*	53.313	47.82	46.34	58.78	50.18	47.60	67.60	54.91	50.56
	T. Sh_{avg}	48.2	80.09	99.74	52.85	86.37	107.36	60.65	98.9	122.82
HNC02	*T. Nu_{avg}*	52.65	47.28	45.84	58.80	50.22	47.63	67.64	54.98	50.62
	T. Sh_{avg}	47.41	78.78	98.10	52.82	86.37	107.37	60.64	98.91	122.85
HNC03	*T. Nu_{avg}*	52.77	47.39	45.95	58.93	50.30	47.73	67.78	55.06	50.71
	T. Sh_{avg}	47.45	78.83	98.16	52.86	86.42	107.42	60.67	98.95	122.89

fluids. Results support that the thermal transport rate for N= 1 and Le= 1 is minimized for Al_2O_3-EG nanofluid but maximized for HNC01 with an enhancement of 3.7 %. For N=4, the HT enhancement is obtained for HNC03 with an amount of 2.6 %. The Al_2O_3-EG nano-coolant demonstrates the lowest HT rates compared to other working fluids in the present study. At the same time, HNC03 emerges as the most promising fluid for thermal transport for higher values of N, exhibiting a remarkable enhancement of 2.57 % in HT rate for Le=1 and 3.11 % for Le=10 while N=4. Additionally, increasing the N from 1 to 4 consistently leads to increased HT and MT, irrespective of the constant value of Le.

6.3. Development of ANN architecture

In implementing the Artificial Neural Network (ANN) methodology, we systematically trained the model using numerical simulation data for nanofluid variations (comprising MWCNT, Al_2O_3, CuO, and EG 30 %) across a range of critical parameters. These parameters include the Rayleigh number (Ra), Buoyancy ratio (N), Lewis number (Le), and volume fractions of MWCNT (ϕ_{MWCNT}), CuO (ϕ_{CuO}), and Al_2O_3 (ϕ_{Al2O3}). To optimize ANN performance, we explored various innovative architectures. The selection process involves evaluating the accuracy of different architectures. The chosen architecture, depicted in Fig. 9, consists of 5 layers with 3 hidden layers arranged in a sequence of 6-50-100-50-2 nodes. This architecture is strategically designed to enhance accuracy by jointly training the model to predict $T.\ Nu_{avg}$ and $T.\ Sh_{avg}$. The inclusion of hidden layers aids in capturing intricate relationships within the data. Table 7 presents a comparative analysis of various neural network architectures, focusing on their testing accuracy, number of parameters, R^2 values for $T.\ Nu_{avg}$ and $T.\ Sh_{avg}$, and mean squared error (MSE). The architectures evaluated include 6-50-2, 6-50-100-2, and 6-50-100-50-2. Among these, the 6-50-100-50-2 architecture demonstrates exceptional performance, achieving an R^2 of 99.97 % for $T.\ Nu_{avg}$ and 99.96 % for $T.\ Sh_{avg}$, along with the lowest MSE of 0.8923.

Despite having the highest number of parameters (10,602), this architecture achieves near-perfect accuracy, suggesting that its increased complexity enables it to capture underlying data patterns effectively. The decision to select the 6-50-100-50-2 architecture is further supported by its ability to minimize errors while maintaining remarkably high accuracy, making it the most dependable model for this study.

Table 7
Identifying the best neural network architecture based on testing accuracy.

ANN (Input-hidden-output)	Total parameter	R^2 for total Nu_{avg}	R^2 for Total Sh_{avg}	MSE
6–50–2	452	98.22 %	98.10 %	49.1174
6–50–100–2	5,652	99.89 %	99.92 %	2.1578
6–50–100–50–2	10,602	99.97 %	99.96 %	0.8923

6.4. ANN training and prediction process

A simulation dataset was created to analyze controlling and hybrid nanofluids, comprising a total of 4,104 data combinations. This dataset includes six distinct attributes (Ra, N, Le, ϕ_{MWCNT}, ϕ_{Al2O3}, and ϕ_{CuO}) as inputs, generating two outputs ($T.\ Nu_{avg}$, $T.\ Sh_{avg}$). Within this dataset, 20 % of the data is allocated for validation, while the remaining portion is used for training. The efficacy of the developed ANN model is evaluated using an entirely new CuO-Al_2O_3-EG30 % hybrid nanofluid containing 2.67 % CuO and 1.33 % Al_2O_3 nanoparticles. Notably, the specific hybrid nanofluid used for evaluation was not part of the training dataset. The test dataset independently assesses the model's generalization abilities, consisting of 684 data combinations. Fig. 10 illustrates the training and validation loss of an Artificial Neural Network (ANN) model across 200 epochs. The y-axis depicts the Mean Square Error (MSE) on a logarithmic scale, while the x-axis indicates the number of epochs. The training and validation losses start at high values and decrease rapidly during the early epochs, demonstrating the model's quick learning. As the training progresses, the rate of improvement slows down, and both losses converge to approximately 10^{-4} by the end of the training. The proximity of the training and validation loss curves suggests that the model generalizes well without overfitting. In Fig. 11, the error histogram from the test dataset shows that the model performs effectively for $T.\ Nu_{avg}$ and $T.\ Sh_{avg}$. Both distributions are centered near zero, indicating minimal bias. The $T.\ Nu_{avg}$ exhibits a tightly clustered distribution, reflecting high precision with most errors within a narrow range. While showing a slightly broader spread, the $T.\ Sh_{avg}$ demonstrates the model's adaptability to varied inputs. Overall, the model is accurate and versatile, handling different scenarios with reliability.

6.5. Comparison between various predicting models

Before delving into the approach of artificial neural network (ANN)

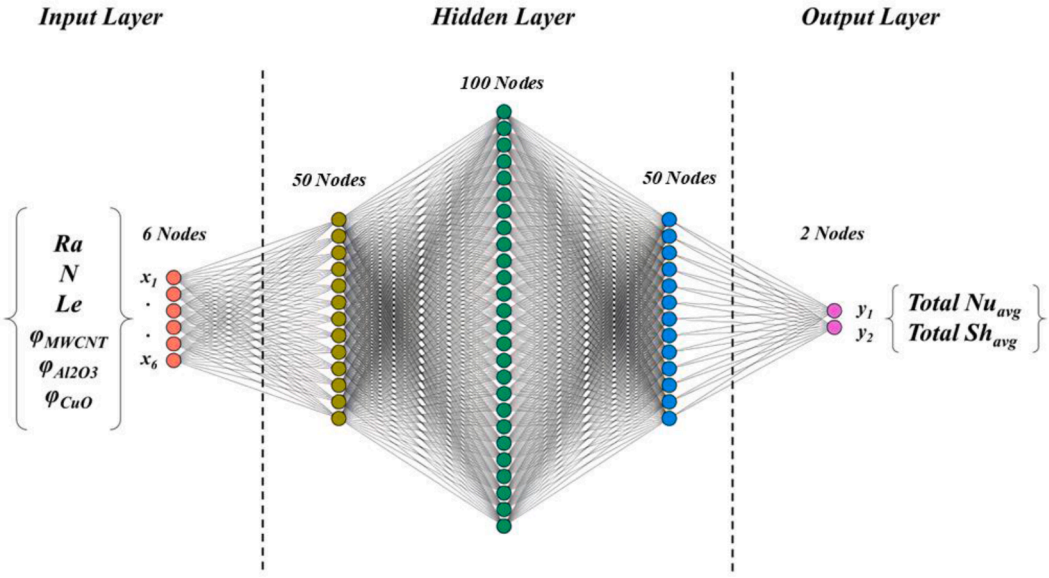

Fig. 9. Architecture of ANN model (6-50-100-50-2).

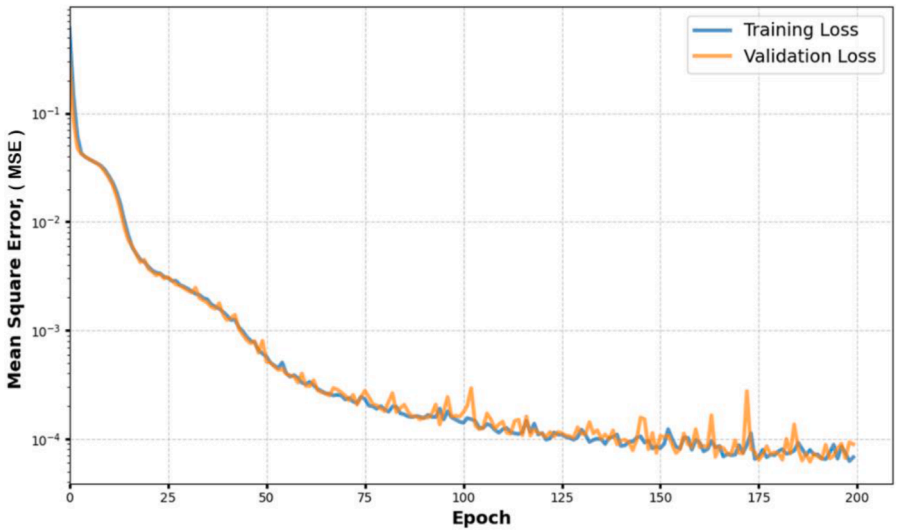

Fig. 10. Training graph on mean epoch.

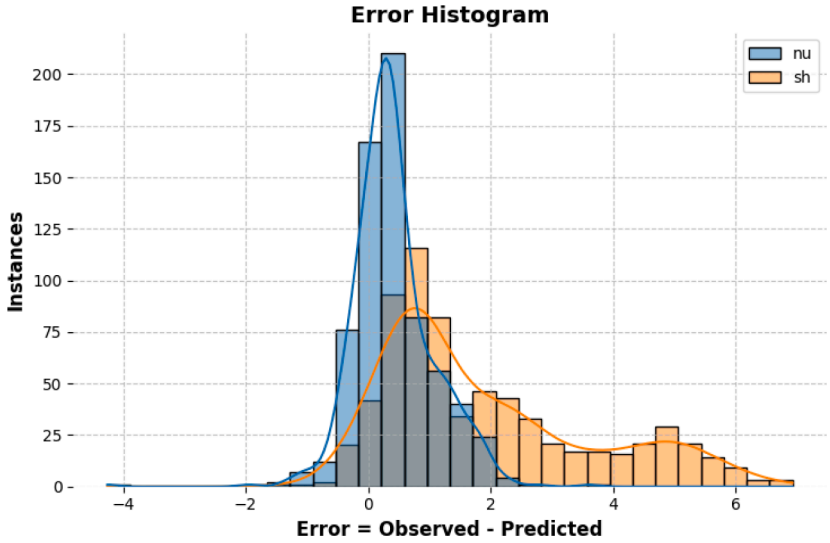

Fig. 11. Error Histogram on the testing dataset.

in our current study, we thoroughly analyzed several machine learning models (MLM) to ensure that the selected model could accurately predict the *T. Nu*$_{avg}$ and *T. Sh*$_{avg}$. To evaluate the model selection, we chose four error metrics: Mean Square Error (MSE), Mean Average Error (MAE), Root Mean Square Error (RMSE), and R^2. The findings in Table 8 unambiguously support the suitability of using ANN as a reliable model for accurately predicting *T. Nu*$_{avg}$ and *T. Sh*$_{avg}$, with a Mean Square Error of 0.89223. The adjusted R^2 value indicates the precision of the results compared to the actual values.

Table 8
Comparing ANN with other existing models.

Model	Mean square error	Mean average error	RMSE	R^2
K-Nearest neighbour regressor	243.7407	11.7762	15.1284	90.22 %
Decision tree regressor	2.1140	0.8460	1.44780	99.89 %
Random forest regressor	1.1462	0.6523	1.06814	99.94 %
ANN (present model)	0.8923	0.6354	0.9446	99.96 %

6.6. *ANN feature on estimating Total Nu*$_{avg}$ *& Total Sh*$_{avg}$

This section explores the qualitative performance of ANN implementation on the large data sets generated from the present numerical simulations. In this regard, plots of Figs. 12 and 13 illustrate how *T. Nu*$_{avg}$ and *T. Sh*$_{avg}$ of one mono nano-coolant (MWCNT-EG) and two hybrid nano-coolants (HNC01 and HNC02) from six training fluids, as mentioned in Table 1, change for various *N* values (1, 2, and 4) as *Le* values (1 to 10). The results show that it consistently decreases with increasing the thermal diffusivity by the values of *Le* for all *Ra* cases. As discussed earlier, strengthening the thermal buoyancy force over the solutal one by the values of *N* for each case of *Ra* boosts the HT rate as aided by the solutal buoyancy force. It is notable to observe that for each nano-coolant, increasing the convective force with the values of *Ra* significantly enhances the T. Nuavg. The results also exhibit the accuracy of an ANN output in estimating *T. Nu*$_{avg}$. In Figs. 12 and 13, solid lines represent CFD simulated results, while dashed lines represent ANN. The ANN outputs successfully estimate the trend of *T. Nu*$_{avg}$ features obtained from the CFD results across all parameter variations. However,

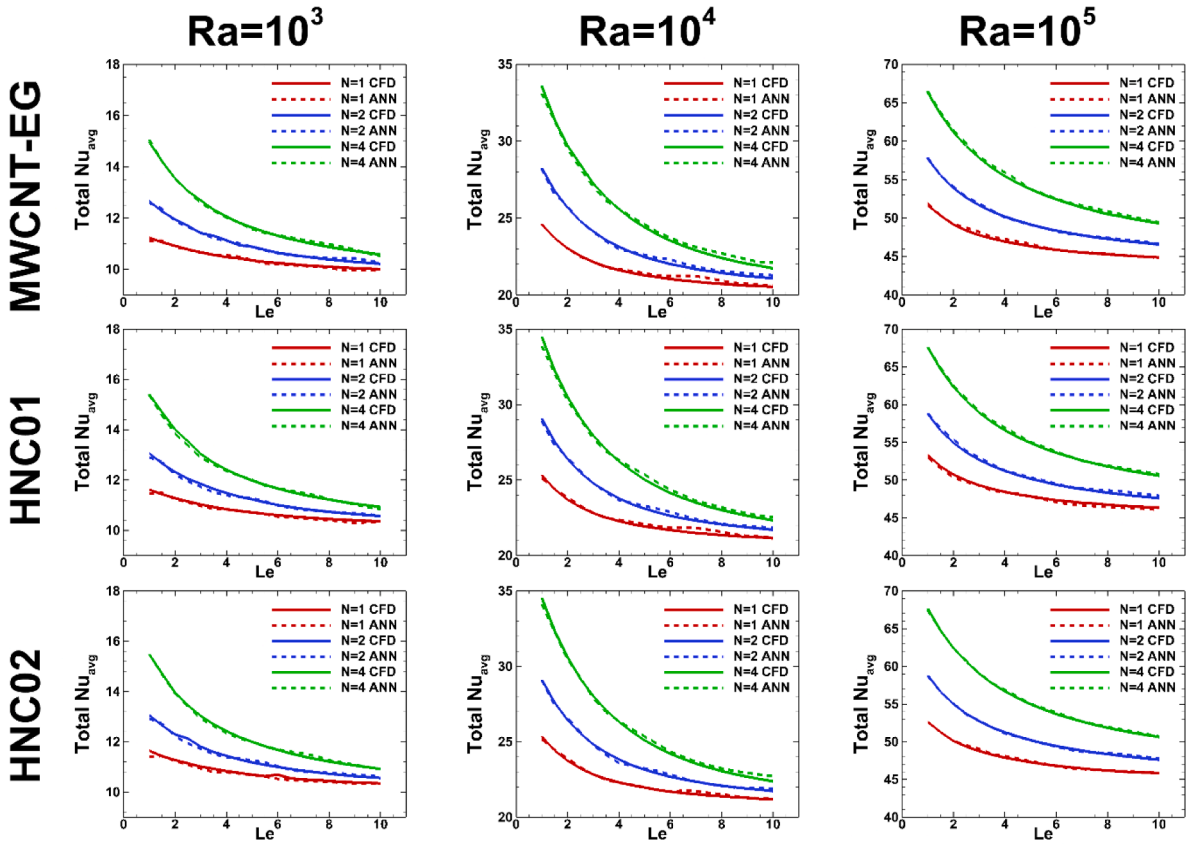

Fig. 12. CFD-ANN comparison of *T.* Nuavg vs.Le for various nano-coolants and Ra-values with N= 1, 2, 4.

some inconsistency was noted when Ra=10^4, with the ANN results deviating from the CFD results for N, resulting in a maximum percentage error of 11 % for $Le > 5$. These findings provide valuable insights into the reliability of the ANN model in predicting HT characteristics. Results in Fig. 13 show that *T.* Sh_{avg} tends to boost with increasing the values of Le as the solutal boundary layer gets thinner by weakening the solutal diffusivity. At Le=1, the temperature and concentration boundary layer thicknesses are equal, resulting in lower MT than higher Le values. Furthermore, when N=1, there is an equal and positive impact on enhancing the *T.* Sh_{avg} from both thermal and solutal buoyancy forces. Additionally, an increase in Ra further amplifies *T.* Sh_{avg} due to the strengthening of the convective action of the flow. Our innovative artificial neural network (ANN) model structure showcases its ability to replicate the behavior of solutal exchange rate *T.* Sh_{avg} with varying parameter values. Despite slight variances, the majority of the ANN model results closely align with the computational fluid dynamics (CFD) results, which validates the effectiveness of this novel ANN architecture.

6.7. ANN prediction on total Nu_{avg} & Sh_{avg}

The developed ANN architecture implemented in the present study has estimated the trained data for various training fluids. Therefore, the present section shows the qualitative and quantitative performance of the ANN modeling to predict the HT and MT characteristics of nanofluids under a new circumstance, including novel fluid types with diverse compositions and varying percentages of nanoparticle volume. Consequently, the performance of the constructed ANN model was assessed using a newly introduced hybrid nanofluid termed Al_2O_3-CuO-EG30 %, which consisted of 1.33 % Al_2O_3 and 2.67 % CuO nanoparticles and was not utilized during ANN model training. This fluid was introduced to test the model's robustness. Fig. 14 illustrates the *T.* Nu_{avg} and *T.* Sh_{avg} values for different Le and N. The model demonstrated its potential in the test fluid by accurately predicting the features of *T.* Nu_{avg} and *T.* Sh_{avg} for a Rayleigh number $Ra = 10^4$as for the choice of interest. Table 9 compares the ANN predictions with results from simulations for the average *T. Nuavg* and *T. Shavg* across different values of Le and N for a quantitative observance of the ANN prediction. Although all results are not shown, the ANN model closely replicated the CFD results across all *Ra* values ranging from 10^3 to 10^5, with *T. Nuavg* deviations range within 1–2 %, and *T. Shavg* deviations range within 2–3 %, even at Ra= 10^5, where convective effects are strong enough. The N, which reflects the ratio of thermal to solutal buoyancy forces, also influenced the results, with the ANN accurately capturing the variations in *T.* Nu_{avg} and *T.* Sh_{avg} as N increased from 1 to 4. Similarly, changes in Le, which represents the ratio of thermal to mass diffusivity, were well predicted by the ANN, showing consistent trends with the CFD results. The model's ability to generalize across different Ra, Le, and N values validates its effectiveness in handling complex, coupled thermo-solutal behaviors in nanofluids. Importantly, the ANN model proved capable of generalizing to new fluid compositions, such as the Al_2O_3-CuO-EG hybrid nanofluid, confirming its reliability for predicting heat and mass transfer characteristics in systems that were not part of the initial training data. This investigation supports the ANN modeling as a valuable tool for reducing the computational costs associated with traditional CFD simulations, especially in practical applications such as designing and optimizing thermal management systems that utilize nanofluids.

6.8. Cost effectiveness of ANN model vs FEM simulation

The numerical simulation of the training data using the finite element method (FEM) on a workstation equipped with a 12th Gen Intel (R) Core (TM) i5-12400, 2.50 GHz processor, and 96.0GB of RAM took approximately 36 h. Subsequently, the simulation data was utilized to

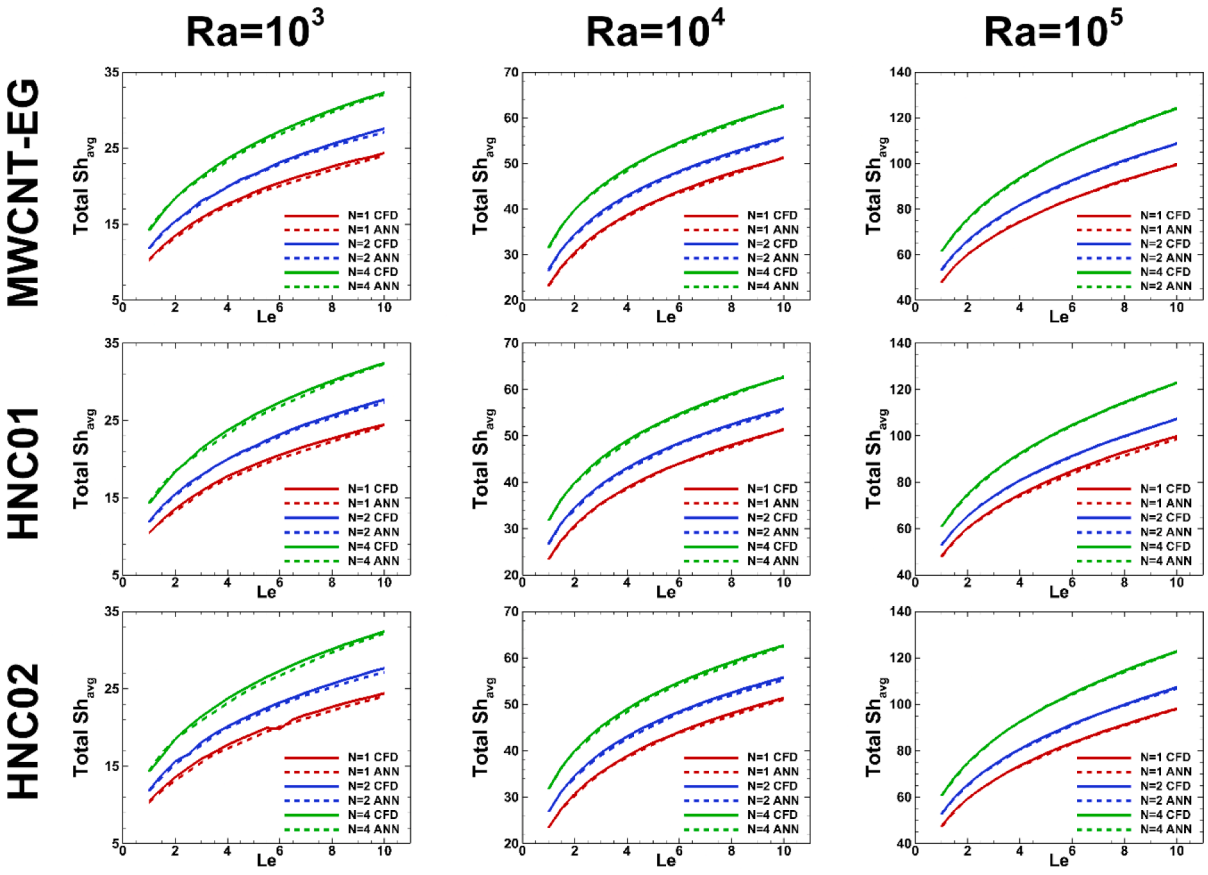

Fig. 13. CFD-ANN comparison of T. Sh_{avg} vs. Le for various nano-coolants and Ra-values with N= 1, 2, 4.

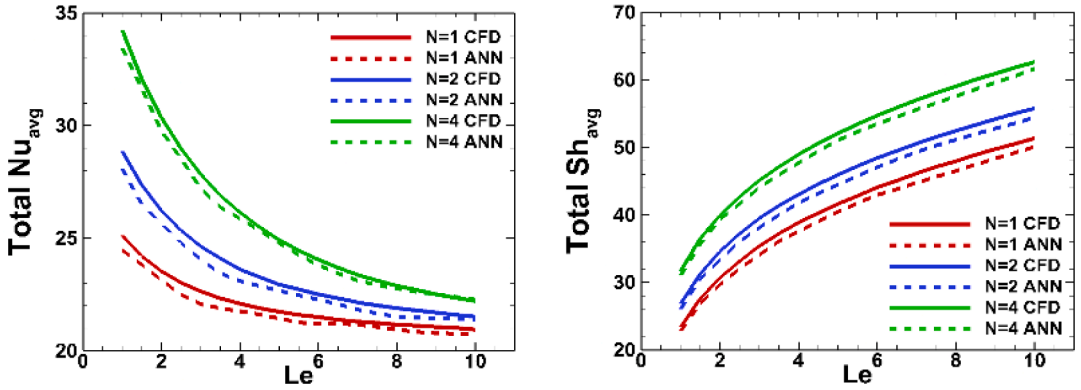

Fig. 14. CFD-ANN comparison on T. Nuavg and T. Shavg in varied Le for HNC04 fluid at N= 1, 2, 4 and Ra= 10^4.

develop an innovative Artificial Neural Network (ANN) model for the same problem, employing the same computational resources. The development of the ANN model, utilizing in-house Python code, involved approximately one hour of training. Post-training, the ANN model demonstrated the capability to provide real-time predictions with high accuracy in seconds, signifying a substantial advancement over the resource-intensive FEM-based simulations. To validate the effectiveness of the ANN model, it was tested using HNC 04, a dataset not included in the training data. In contrast, generating heat and mass transfer findings for HNC 04, with various governing parameter values using FEM, took approximately 6 hours. As previously mentioned, the developed ANN model rapidly provided predictions for the same input features in seconds with exceptional accuracy, highlighting the computational efficiency of ANN compared to FEM. The study's outcomes validate the ability of ANN to reduce computational time and associated expenses in computational studies.

7. Conclusion

This study explores the double-diffusive natural convection emanating from three heated chips placed within an enclosure with two vertical cold sides. The investigation incorporates a wide range of nanocoolants for convective medium, including MWCNT, Al_2O_3, and CuO nanoparticles with varying weight percentages in the base fluid ethylene glycol (30:70). The study systematically investigates the influence of critical parameters such as Ra, N, and Le on the heat transfer (HT) and mass transfer (MT). The data generated serves as a robust training dataset for existing machine learning (ML) and Artificial Neural

Table 9
ANN prediction on T. Nuavg and T. Shavg for HNC04 fluid at various *N* and *Le* while $Ra=10^5$.

	N= 1		*N*= 2		*N*=4	
	CFD	ANN (Δ%)	CFD	ANN (Δ%)	CFD	ANN (Δ%)
	Total Nu_{avg}					
Le= 2	50.163	49.300 (1.72 %)	55.009	54.169 (1.53 %)	62.469	61.419 (1.68 %)
Le= 4	47.894	47.210 (1.43 %)	51.21	50.176 (2.02 %)	56.609	55.980 (1.11 %)
Le= 6	46.805	45.822 (2.10 %)	49.366	48.407 (1.94 %)	53.520	52.906 (1.15 %)
Le= 8	46.214	45.308 (1.96 %)	48.261	47.458 (1.66 %)	51.576	51.023 (1.07 %)
Le= 10	45.802	44.869 (2.03 %)	47.517	46.706 (1.71 %)	50.340	49.716 (1.24 %)
	Total Sh_{avg}					
Le= 2	60.152	58.650 (2.50 %)	66.338	64.542 (2.71 %)	75.898	74.247 (2.17 %)
Le= 4	74.571	72.621 (2.61 %)	81.940	80.021 (2.34 %)	93.833	91.746 (2.22 %)
Le= 6	84.727	82.406 (2.74 %)	92.901	90.178 (2.93 %)	106.253	103.479 (2.61 %)
Le= 8	92.905	89.972 (3.16 %)	101.595	99.155 (2.40 %)	116.014	113.229 (2.40 %)
Le= 10	99.642	97.497 (2.15 %)	108.852	106.346 (2.30 %)	124.353	122.137 (1.78 %)

Network (ANN) models. Key findings from the study include:

- Heat and mass transfer increase with increasing the buoyancy forces by the values of *Ra*, peaking at $Ra= 10^5$.
- Increasing the convective buoyancy forces (*Ra*) enhances the HT from the centrally positioned heated chips towards the greater contribution to the *T.* Nu_{avg}.
- *T.* Nu_{avg} is highest at lower thermal diffusivity (*Le*= 1) and highest buoyancy ratio (*N*= 4) for all coolants.
- *T.* Sh_{avg} shows it's enhanced MT by increasing both *Le* and *N* for all nano-coolant variations.
- HNC03 outperforms other nanocoolants, improving heat transfer by 3.11 % for *N*= 4 and *Le*= 10.
- The optimal ANN model (6-50-100-50-2) accurately predicts heat and mass transfer with $R^2= 0.99982$ and MSE= 0.8923.
- The ANN model closely replicated the test fluid results from CFD across all *Ra* values, with *T. Nuavg* deviations range within 1–2 %, and *T. Shavg* deviations range within 2–3 % when $Ra= 10^5$.

The study highlights the computational efficiency of ANN, emphasizing its potential as a valuable tool to reduce computation time and costs in complex simulations. To fully realize the potential of our study, it is essential to acknowledge its limitations and consider future perspectives:

- The ANN model optimizes *Ra, N, Le*, and coolant combinations for better heat and mass transfer. Future research can improve predictions by combining ANNs with genetic algorithms, especially for managing hybrid and regular nanocoolants.
- It is essential to recognize that the selected architecture may have limitations in terms of computational costs for real-time applications. Investigating alternative approaches or employing dimensionality reduction techniques to address this challenge would be prudent.
- Expanding the study to higher *Ra* values beyond 10^3 to 10^5 could offer new insights into extreme conditions.

In summary, the integration of ANN modeling with diverse parameter variations and validation against CFD results underscores its effectiveness in accurately predicting heat and mass transfer characteristics. This advancement contributes significantly to the ongoing progress in computational fluid dynamics studies.

Funding

The North South University CTRG research grant (Grant No.: CTRG-23-SEPS-31) is acknowledged for supporting the RA ship in conducting this research.

CRediT authorship contribution statement

Tawsif Mahmud: Writing – original draft, Visualization, Validation, Software, Methodology, Investigation, Formal analysis. **Jiaul Haque Saboj:** Visualization, Validation, Software, Investigation. **Preetom Nag:** Writing – review & editing, Supervision, Software, Resources, Project administration, Investigation, Funding acquisition, Formal analysis, Conceptualization. **Goutam Saha:** Writing – review & editing, Supervision. **Bijan K. Saha:** Writing – review & editing, Supervision.

Declaration of competing interest

The authors declare that they have no known competing financial interests or personal relationships that could have appeared to influence the work reported in this paper.

Data availability

Data will be made available on request.

References

[1] J.A. Weaver, R. Viskanta, Natural convection in binary gases due to horizontal thermal and solutal gradients, ASME. J. Heat Transf. 113 (1) (1991) 141–147.
[2] J.A. Esfahani, V. Bordbar, Double diffusive natural convection heat transfer enhancement in a square enclosure using nanofluids, ASME. J. Nanotechnol. Eng. Med 2 (2) (2011) 021002.
[3] V.A.F. Costa, Double-diffusive natural convection in parallelogrammic enclosures, Int. J. Heat. Mass Transf. 47 (14–16) (2004) 2913–2926.
[4] M.A. Teamah, W.M. El-Maghlany, Numerical simulation of double-diffusive mixed convective flow in rectangular enclosure with insulated moving lid, Int. J. Therm. Sci. 49 (9) (2010) 1625–1638.
[5] H. Xu, R. Xiao, F. Karimi, M. Yang, Y. Zhang, Numerical study of double diffusive mixed convection around a heated cylinder in an enclosure, Int. J. Therm. Sci. 78 (2014) 169–181.
[6] Y. Xia, J. Chen, Direct numerical simulation of double diffusive natural convection in a closed mixture cavity heated from below, Therm. Sci. 27 (5) (2023) 4261–4275. Part B.
[7] M. Moderres, T. Benmalek, A. Sofiane, A. Ghezal, S. Abboudi, A. Benbrik, Double-diffusive natural convection in a cavity with an inner cylinder wrapped by a porous layer, Therm. Sci. 26 (2) (2022) 1841–1853. Part C.
[8] M.S. Aghighi, A. Ammar, H. Masoumi, Double-diffusive natural convection of Casson fluids in an enclosure, Int. J. Mech. Sci. 236 (2022) 107754.
[9] R. Parveen, A.K. Hussein, T.R. Mahapatra, M. Al-Thamir, A. Abidi, M.B. Ben Hamida, R.Z. Homod, F.L. Rashid, MHD double diffusive mixed convection and heat generation /absorption in a lid-driven inclined wavy enclosure filled with a ferrofluid, Int. J. Thermofluids 22 (2024) 100698.
[10] A. Bouras, M. Djezzar, H. Naji, C. Ghernoug, Numerical computation of double-diffusive natural convective flow within an elliptic-shape enclosure, Int. Commun. Heat Mass Transf. 57 (2014) 183–192.
[11] M.S. Aghighi, A. Ammar, H. Masoumi, Double-diffusive natural convection of Casson fluids in an enclosure, Int. J. Mech. Sci. 236 (2022) 107754.
[12] S. Choi, J. Eastman, Enhancing thermal conductivity of fluids with nanoparticles, Am. Soc. Mech. Eng. Fluids Eng. Div. 231 (1995) 99–105.
[13] Y. Xuan, Q. Li, Heat transfer enhancement of nanofluids, Int. J. Heat. Fluid. Flow. 21 (1) (2000) 58–64.
[14] J.A. Eastman, S.U.S. Choi, S. Li, W. Yu, L.J. Thompson, Anomalously increased effective thermal conductivities of ethylene glycol-based nanofluids containing copper nanoparticles, Appl. Phys. Lett. 78 (6) (2001) 718–720.
[15] T. Armaghani, M.S. Sadeghi, A.M. Rashad, M.A. Mansour, A.J. Chamkha, A. S. Dogonchi, H.A. Nabwey, MHD mixed convection of localized heat source/sink in an al2o3-cu/water hybrid nanofluid in L-shaped cavity, Alex. Eng. J. 60 (3) (2021) 2947–2962.
[16] M.I. Hasan, H.L. Tbena, Enhancing the cooling performance of micro pin fin heat sink by using the phase change materials with different configurations, in: International Conference on Advance of Sustainable Engineering and Its Application (ICASEA), 2018.

[17] Y. Abudllah, Z. Arifin, D. Danardono Dwi Prija Tjahjana, S. Suyitno, M.R. Aulia Putra, Analysis of the copper and aluminum heat sinks addition to the performance of photovoltaic panels with CFD modelling, in: 1st International Conference on Information Technology, Advanced Mechanical and Electrical Engineering (ICITAMEE), 2020.
[18] P. Selvakumar, S. Suresh, Use of Al2O3–Cu/water hybrid nanofluid in an electronic heat sink, IEEE Trans. Compon. Packag. Manuf. Technol. 2 (10) (2012) 1600–1607.
[19] H.T. Kadhim, A. Al-Manea, A.N. Al-Shamani, T. Yusaf, Numerical Analysis of hybrid nanofluid natural convection in a wavy walled porous enclosure: Local thermal non-equilibrium model, Int. J. Thermofluids 15 (2022) 100190.
[20] M.M. Haque, M.S. Alam, Natural convective heat transfer of al2o3-cu/water hybrid nanofluid in a rectotrapezoidal enclosure under the influence of periodic magnetic field, Int. J. Thermofluids 22 (2024) 100661.
[21] E. Elshazly, A.A. Abdel-Rehim, I. El-Mahallawi, Thermal performance enhancement of evacuated tube solar collector using MWCNT, Al2O3, and hybrid MWCNT/Al2O3nanofluids, Int. J. Thermofluids 17 (2023) 100260.
[22] M. Baghbanzadeh, A. Rashidi, D. Rashtchian, R. Lotfi, A. Amrollahi, Synthesis of spherical silica/multiwall carbon nanotubes hybrid nanostructures and investigation of thermal conductivity of related nanofluids, Thermochim. Acta 549 (2012) 87–94.
[23] T. Theres Baby, R. Sundara, Synthesis of silver nanoparticle decorated multi-walled carbon nanotubes-graphene mixture and its heat transfer studies in nanofluid, AIP. Adv. 3 (1) (2013).
[24] A. Filali, L. Khezzar, H. Semmari, O. Matar, Application of artificial neural network for mixed convection in a square lid-driven cavity with double vertical or horizontal oriented rectangular blocks, Int. Commun. Heat Mass Transf. 129 (2021) 105644.
[25] Y.M. Seo, K. Luo, M.Y. Ha, Y.G. Park, Direct numerical simulation and artificial neural network modeling of heat transfer characteristics on natural convection with a sinusoidal cylinder in a long rectangular enclosure, Int. J. Heat. Mass Transf. 152 (2020) 119564.
[26] M. Afrand, D. Toghraie, N. Sina, Experimental study on thermal conductivity of water-based FE3O4 nanofluid: Development of a new correlation and modeled by artificial neural network, Int. Commun. Heat Mass Transf. 75 (2016) 262–269.
[27] M. Hemmat Esfe, S. Esfandeh, S. Saedodin, H. Rostamian, Experimental evaluation, sensitivity analyzation and ann modeling of thermal conductivity of Zno-MWCNT/EG-water hybrid nanofluid for engineering applications, Appl. Therm. Eng. 125 (2017) 673–685.
[28] S. Rostami, D. Toghraie, M.A. Esfahani, M. Hekmatifar, N. Sina, Predict the thermal conductivity of SiO_2/water–ethylene glycol (50:50) hybrid nanofluid using artificial neural network, J. Therm. Anal. Calorim. 143 (2) (2021) 1119–1128.
[29] M.R. Faridzadeh, D. Toghraie Semiromi, A. Niroomand, Analysis of laminar mixed convection in an inclined square lid-driven cavity with a nanofluid by using an artificial neural network, Heat. Transf. Res. 45 (4) (2014) 361–390.
[30] J.S. Xia, M. Khaje Khabaz, I. Patra, I. Khalid, J.R.N. Alvarez, A. Rahmanian, S. A. Eftekhari, D. Toghraie, Using feed-forward perceptron Artificial Neural Network (ANN) model to determine the rolling force, power and slip of the tandem cold rolling, ISA Trans. 132 (2023) 353–363.
[31] X. Yang, A. Boroomandpour, S. Wen, D. Toghraie, F. Soltani, Applying Artificial Neural Networks (ANNs) for prediction of the thermal characteristics of water/ethylene glycol-based mono, binary and ternary nanofluids containing MWCNTs, Titania, and zinc oxide, Powder. Technol. 388 (2021) 418–424.
[32] H. Boulechfar, F. Berrahil, A. Boulmerka, A. Filali, M. Djezzar, Double diffusive buoyancy-driven flow in a fluid-saturated elliptical annulus with a neural network-based prediction of heat and mass transfer, Heat Transf. 52 (6) (2023) 4199–4226.
[33] P.A. Costa Rocha, S.J. Johnston, V. Oliveira Santos, A.A. Aliabadi, J.V. Thé, B. Gharabaghi, Deep neural network modeling for CFD simulations: Benchmarking the Fourier neural operator on the lid-driven cavity case, Appl. Sci. 13 (5) (2023) 3165.
[34] D.K. Mandal, N. Biswas, N.K. Manna, D.K. Gayen, R.S. Gorla, A.J. Chamkha, Thermo-fluidic transport process in a novel M-shaped cavity packed with non-Darcian porous medium and hybrid nanofluid: Application of artificial neural network (ANN), Phys. Fluids, 34 (3) (2022) 033608.
[35] F. Bouzeffour, Artificial neural network-based modeling for the prediction of heat and mass transfer coefficient of the adiabatic liquid desiccant system, J. Renew. Energies 25 (2) (2022) 157–167.
[36] R.J. Varela, S. Yamaguchi, N. Giannetti, K. Saito, M. Harada, H. Miyauchi, General correlations for the heat and mass transfer coefficients in an air-solution contactor of a liquid desiccant system and an experimental case application, Int. J. Heat. Mass Transf. 120 (2018) 851–860.
[37] V. Verma, R. Nath, R. Tarodiya, Heat transfer prediction for radiant floor heating/cooling systems using artificial neural network (ANN), Heat Transf. 52 (4) (2023) 3135–3152.
[38] A. Kargar, B. Ghasemi, S.M. Aminossadati, An artificial neural network approach to cooling analysis of electronic components in enclosures filled with nanofluids, ASME. J. Electron. Packag. 133 (1) (2011) 011010.
[39] H.A. Prince, A. Ghosh, M.M. Siam, M.A. Mamun, AI predicts MHD double-diffusive mixed convection and entropy generation in hybrid-nanofluids for different magnetic field inclination angles by ann, Int. J. Thermofluids 19 (2023) 100383.
[40] M.H. Esfe, S.A. Eftekhari, M. Hekmatifar, D. Toghraie, A well-trained artificial neural network for predicting the rheological behavior of MWCNT–Al2O3 (30–70%)/oil SAE40 hybrid nanofluid, Sci. Rep. 11 (1) (2021) 17696.
[41] M.H. Esfe, R. Esmaily, M.K. Khabaz, A. Alizadeh, M. Pirmoradian, A. Rahmanian, D. Toghraie, A novel integrated model to improve the dynamic viscosity of MWCNT-Al2O3 (40:60)/Oil 5W50 hybrid nano-lubricant using artificial neural networks (ANNs), Tribol. Int. 178 (2023) 108086.
[42] P. Nag, Md.M. Molla, Double-diffusive natural convection of non-newtonian nanofluid considering thermal dispersion of nanoparticles in a vertical wavy enclosure, AIP. Adv. 11 (9) (2021).
[43] T. Mahmud, T. Chowdhury, P. Nag, M.M. Molla, Entropy production associated with magnetohydrodynamics (MHD) thermo-solutal natural convection of non-Newtonian MWCNT-SiO2-EG hybrid nano-coolant, Heliyon. 10 (15) (2024) e35523.
[44] A. Mourad, A. Aissa, F. Mebarek-Oudina, W. Jamshed, W. Ahmed, H.M. Ali, A. M. Rashad, Galerkin finite element analysis of thermal aspects of Feo-MWCNT/water hybrid nanofluid filled in wavy enclosure with uniform magnetic field effect, Int. Commun. Heat Mass Transf. 126 (2021) 105461.
[45] S. Acharya, S.K. Dash, Natural convection in a cavity with undulated walls filled with water-based non-newtonian power-law cuo–water nanofluid under the influence of the external magnetic field, Numer. Heat Transf. Part A Appl. 76 (7) (2019) 552–575.
[46] H. Masuda, A. Ebata, K. Teramae, N. Hishinuma, Alteration of thermal conductivity and viscosity of liquid by dispersing ultra-fine particles. dispersion of Al2O3, SiO2 and TiO2 ultra-fine particles, Netsu Bussei 7 (4) (1993) 227–233.
[47] M. Corcione, Empirical correlating equations for predicting the effective thermal conductivity and dynamic viscosity of nanofluids, Energy Convers. Manage. 52 (1) (2011) 789–793.
[48] T. Mahmud, T. Chowdhury, P. Nag, M.M. Molla, Entropy production associated with magnetohydrodynamics (MHD) thermo-solutal natural convection of non-Newtonian MWCNT-SiO2-EG hybrid nano-coolant, Heliyon. 10 (15) (2024) e35523.
[49] F. Acito, k nearest neighbors. Predictive Analytics with KNIME, Springer, 2023, pp. 209–227.
[50] S. Das, A.K. Jha, R. Johnsan, C.S. Bestha, V. Teja Reddy, Prediction of heat transfer performance of heat pipe using machine learning approach, in: Proceedings of the 1st International Conference on Fluid, Thermal and Energy Systems, Springer Nature, Singapore, 2024, pp. 97–107.
[51] G. N, P. Jain, A. Choudhury, P. Dutta, K. Kalita, P. Barsocchi, Random forest regression-based machine learning model for accurate estimation of fluid flow in curved pipes, Processes 9 (11) (2021) 2095.
[52] J.A. Weaver, R. Viskanta, Natural convection in binary gases due to horizontal thermal and solutal gradients, ASME. J. Heat Transfer 113 (1) (1991) 141–147.
[53] M. Paroncini, F. Corvaro, Natural convection in a square enclosure with a hot source, Int. J. Therm. Sci. 48 (9) (2009) 1683–1695.
[54] K.M. Rahim, J. Ahmed, P. Nag, Md.M. Molla, Lattice Boltzmann simulation of natural convection and heat transfer from multiple heated blocks, Heat Transf. 49 (4) (2020) 1877–1894.
[55] C.J. Ho, W.K. Liu, Y.S. Chang, C.C. Lin, Natural convection heat transfer of alumina-water nanofluid in Vertical Square Enclosures: an experimental study, Int. J. Therm. Sci. 49 (8) (2010) 1345–1353.
[56] A.I. Alsabery, M.A. Sheremet, A.J. Chamkha, I. Hashim, MHD convective heat transfer in a discretely heated square cavity with conductive inner block using two-phase nanofluid model, Sci. Rep. 8 (1) (2018).
[57] S.Y. Motlagh, H. Soltanipour, Natural convection of al2o3-water nanofluid in an inclined cavity using Buongiorno's two-phase model, Int. J. Therm. Sci. 111 (2017) 310–320.
[58] I. Sezai, A.A. Mohamad, Double diffusive convection in a cubic enclosure with opposing temperature and concentration gradients, Phys. Fluids 12 (9) (2000) 2210–2223.